Reviewed Preprint
v1 • December 23, 2025
Not revised

Reviewed Preprint
v2 • June 4, 2026
Revised by authors

For correspondence:
guy.tranvannhieu@i2bc.paris-saclay.fr

§ Equal contribution

Competing interests: No competing interests declared

Funding: See page 31

Reviewing editor: Bree Aldridge, Tufts University School of Medicine, United States



# Enteropathogenic *E. coli*-mediated Fast and Coordinated $Ca^{2+}$ responses regulate NF-κB activation

**Fangrui Guo[1,2], Roberto Ornelas Guevara[3], Linda Oussaedine[1,2], Geneviève Dupont[3], Laurent Combettes[1,2,§], Guy Tran Van Nhieu[1,2,§]**

[1]Team "$Ca^{2+}$ signaling and Microbial Infections", Institute for Integrative Biology of the Cell (I2BC), CEA, CNRS UMR9198, Université Paris-Saclay, Gif-sur-Yvette, France • [2]Institut National de la Santé et de la Recherche Médicale, U1280, 91190, Gif-sur-Yvette, France • [3]Unit of Theoretical Chronobiology, Université Libre de Bruxelles, Brussels, Belgium

## eLife Assessment

This study reports **important** advances in our understanding of how enteropathogenic E. coli (EPEC) interacts at the intestinal interface. **Compelling** data describe a novel model of spatially coordinated calcium signaling to modulate NF-kB activation. These findings, which integrate imaging, genetics, and computational modeling, provide a new way to consider host-pathogen interactions in EPEC infections that may lead to improved therapies.

https://doi.org/10.7554/eLife.108953.2.sa3

## Abstract

Enteropathogenic *Escherichia coli* (EPEC) is a major bacterial enteropathogen causing infectious diarrhea among children in developing countries. Here, we found that EPEC induced isolated $Ca^{2+}$ responses in epithelial cells, triggered by extracellular ATP (eATP). These responses were dependent on type III secretion (T3S) and down-regulated by the bacterial secreted protease EspC, consistent with eATP released by the T3S translocon pore-forming activity in host membranes. By performing high speed $Ca^{2+}$ imaging, we uncovered that at the onset of infection, low eATP levels triggered $Ca^{2+}$-responses involving the whole cell but showing the small amplitude and fast kinetics usually associated with local $Ca^{2+}$ responses. The findings, supported by theoretical modeling, evocate a conceptual shift whereby low amounts of inositol 1, 4, 5-trisphosphate ($IP_3$) induced by low eATP levels and subsequent moderate $Ca^{2+}$ release enable the fast coordination of $IP_3$ receptor cluster activation throughout the cell. Importantly, these yet undescribed coordinated fast responses occurred over prolonged time periods and defined a cell state with dampened activation of the pro-inflammatory transcriptional activator NF-kB associated with a decrease in its $Ca^{2+}$-dependent O-linked β-N-acetylglucosamine modification.

## Introduction

EPEC are diarrheagenic *E. coli* strains that cause significant morbidity and mortality in children under two years of age. While infection rates have significantly declined in industrialized nations, EPEC remains a major public health concern in low-income countries (Lozer et al., 2013). EPEC form attaching and effacing (A/E) lesions on intestinal epithelial cells and lack the ability to produce Shiga toxins or heat-labile (LT) and heat-stable (ST) enterotoxins (Croxen et al., 2013; Gomes et al., 2016; Hazen et al., 2016). The ability of EPEC to form A/E lesions is determined by the locus of Enterocyte Effacement (LEE), a large genomic pathogenicity island that encodes the essential genetic elements required for this process (Pearson et al., 2016). The LEE region of EPEC (E2348/69) encodes components of the type III secretion system (T3SS), a molecular

apparatus that translocate at least 25 bacterial effector proteins into the host cell. The EPEC type III secretion system (T3SS) consists of a basal body and a needle-like structure, resembling those found in *Salmonella* and *Shigella*, but with a distinct sheath-like extension at the needle tip, primarily composed of EspA, and about ten times longer than the T3SS needles from other bacterial species. This EspA filament acts as a molecular bridge, extending from the bacterium to the host cell membrane, allowing insertion of the EspB and EspD translocon components into the host cell membrane, enabling type III effectors injection in the cell cytosol (Creasey et al., 2003; Monjarás Feria et al., 2012; Sal-Man et al., 2012). Osmoprotection assays suggest that the translocon forms a pore with an internal diameter ranging between 3 to 5 nm, allowing the passage of unfolded effector proteins into the host cell (Chatterjee et al., 2015). However, the T3SS translocon shows weak pore-forming activity during EPEC infection of epithelial cells, presumably because it forms a sealed conduct between the T3SS and host cell membranes (Guignot et al., 2016). EspC, a secreted serine protease from the autotransporter family, targets EspA and EspD and down-regulates pore formation activity associated with cytotoxicity (Guignot et al., 2015). EPEC T3SS effector proteins translocated into host cells lead are responsible for attaching and effacing (A/E) lesions and intimate bacterial adhesion to the host cells associated with the formation of an actin-rich pedestal formation (Chen & Frankel, 2005).

The detection of pathogenic bacteria by intestinal epithelial cells plays an important role in initiating pro-inflammatory responses. Recognition of bacterial surface components by pattern recognition receptors triggers pro-inflammatory signaling pathways involving the transcriptional activator NF-κB and the production of cytokines such as interleukin-8 and tumor necrosis factor-α (TNF-α) (Edwards et al., 2011). However, EPEC suppresses these signaling pathways early in infection through the coordinated action of several T3SS effector proteins. Among the first translocated T3SS effectors, Tir interacts with TNF-α receptor-associated factors (TRAF2 and TRAF6), recruiting the tyrosine phosphatases SHP-1 and SHP-2 (Mills et al., 2008; Ruchaud-Sparagano et al., 2011; Yan et al., 2013). Several non-LEE T3SS effectors, including NleE, NleB, NleH1, NleH2, NleC, and NleD, further contribute to inhibiting NF-κB and MAPK signaling. NleE and NleB stabilize the interaction between NFκB and its inhibitory subunit IκB, preventing its degradation, thereby keeping NFκB in an inactive state. The ability of NleE to inhibit NFκB signaling depends on its S-adenosyl-L-methionine (SAM)-dependent methyltransferase activity (Zhang et al., 2011). NleE-mediated methylation of TAB2/3 prevents IKK activation (Zhang et al., 2011). NleB selectively blocks NFκB activation through GlcNAcylation of the TNF-α receptor (TNFR) adaptor protein and TNFR1-associated death domain (TRADD) (S. Li et al., 2013; Pearson et al., 2013). The T3SS effectors NleH1, NleH2 and NleC also interfere with NFκB nuclear translocation (Gao et al., 2009). NleC specifically cleaves P65 RelA (Giogha et al., 2015; Ruchaud-Sparagano et al., 2011; Yen et al., 2010). Interestingly, NleF has been implicated in the activation of NF-κB, underscoring the complexity of the regulation of inflammation during bacterial infection and suggesting the timing of various T3SS effectors' activity (Pallett et al., 2014).

A similar complexity applies to T3SS effectors regulating cell death and survival pathways during EPEC infection of epithelial cells. Tir was found to elicit a rapid $Ca^{2+}$ influx across the host cell membrane, through the activation of a host plasma membrane $Ca^{2+}$ channel, the mechanosensitive transient receptor potential vanilloid 2 (TRPV2) leading to pyroptosis (Zhong et al., 2022). However, the NleA effector, blocks the delivery of TRPV2 channels to the cell surface, thereby dampening Tir-induced $Ca^{2+}$ influx. The effector NleF also directly binds caspase-4 to inhibit its activity (Zhong et al., 2020). The extrinsic apoptotic pathway is triggered by EPEC pili (Abul-Milh et al., 2001). However, the NleD and NleB effectors inhibit this pathway by cleaving JNK and GlcNAcylating the death domain adaptor proteins TRADD and FADD, respectively (Baruch, Gur-Arie, et al., 2011; Pearson et al., 2013). While EspC prevents cytotoxicity linked to pore-formation by the T3SS translocon during the early EPEC infection phases, it was shown to promote intrinsic apoptosis through increase in intracellular $Ca^{2+}$ and calpain activation (Serapio-Palacios & Navarro-Garcia, 2016).

Central to inflammation and cell death / survival pathways induced by EPEC, bacterial-induced $Ca^{2+}$ signals have been a matter of debate. EPEC infection is known to perturb host $Ca^{2+}$ signaling, but the source and sequence of $Ca^{2+}$ signals during infection remain controversial. EPEC was shown to induce $Ca^{2+}$ influx associated with a loss of mitochondrial membranes permeability leading to cell death (Zhong et al., 2020; Ramachandran et al., 2020; Zhong et al., 2022), but was also reported to trigger $IP_3$-mediated $Ca^{2+}$ release possibly involved in bacterial-induced cytoskeletal rearrangements (Baldwin et al., 1991; Baldwin et al., 1993; Foubister et al., 1994; Bain et al., 1998).

Here, we investigated the characteristics and implications of EPEC-induced $Ca^{2+}$ responses in epithelial cells. We characterized yet undescribed $Ca^{2+}$ signals induced by EPEC and low ATP levels, presenting the fast dynamics and small amplitude of local $Ca^{2+}$ responses but involving large cell area. We found that these responses likely result from the coordination of elementary responses via rapid $Ca^{2+}$-induced $Ca^{2+}$ release over large cell area, challenging generally admitted concepts on $Ca^{2+}$ diffusion. Importantly, we show that these newly described responses have functional implications by dampening the cell ability to respond to inflammatory signals.

# Results

## EPEC induces $Ca^{2+}$ responses that depend on Type III secretion-mediated eATP release

Despite their critical role in cellular processes key to bacterial infection, EPEC-induced $Ca^{2+}$ responses remain to be characterized. We therefore set up to perform a detailed single cell imaging of $Ca^{2+}$ responses elicited by cells infected by EPEC.

As shown in Fig. 1, EPEC induced $Ca^{2+}$ transients often corresponding to a single peak of varying amplitude detected over several minutes, corresponding to 6.2 ± 0.8% (mean ± SEM) of the maximal histamine response (Figs. 1A, B). These $Ca^{2+}$ responses were dependent on a functional T3SS, since they were not observed for the T3SS-deficient *escN* mutant (Figs. 1A, C). Only 40 ± 4.7 % (mean ± SEM) of cells, however, elicited responses when challenged wild-type EPEC at a low multiplicity of infection (MOI) of 20 bacteria per cell, a value that raised to 76 ± 4.8 % (mean ± SEM) when using a high MOI of 80 bacteria per cell (Fig. 1C). In contrast, even at the low MOI, more than 83 % of cells showed actin pedestals, indicating that $Ca^{2+}$ responses were elicited only in a fraction of cells targeted by EPEC-type T3SS (Figs. 1D, E). The frequency of $Ca^{2+}$ responses per cell increased over the incubation time with an average frequency of responses per cell raising by 6.9 to 8.3-fold from the first to the last 30 min of EPEC challenge (Fig. 1F). This increased frequency suggested the accumulation of an agonist in the extracellular medium during the course of the infection triggering $IP_3$-mediated $Ca^{2+}$ release. When pooling all single cell responses, we could observe a steady increase in the average cytosolic $Ca^{2+}$ concentration of the cell population, as previously reported (Ramachandran et al., 2020; Figs. S1B). However, when performing single cell imaging, we did not observe an increase in cytosolic $Ca^{2+}$ basal levels even at high MOI after 2 hours incubation with wild-type bacteria (Fig. S1A).

Together, these results suggest that EPEC induces isolated $Ca^{2+}$ responses that depend on the T3SS for the release of limiting amounts of a $Ca^{2+}$ agonist.

## EPEC-mediated $Ca^{2+}$ responses depend on ATP released in the extracellular medium via the T3SS translocon

In previous works, we showed that the EPEC T3SS translocon forms pores in host cell plasma membranes that were down-regulated by the bacterial secreted serine protease EspC (Guignot et al., 2016). We posit that low amounts of ATP released in the extracellular medium by the T3SS translocon were responsible for the isolated $Ca^{2+}$ responses of reduced amplitude elicited by EPEC. According to this view, by removing T3SS translocons from host cell membranes, EspC would down-regulate EPEC-mediated $Ca^{2+}$ signaling explaining the low ratio of $Ca^{2+}$ responding cells relative to cells forming actin pedestals.

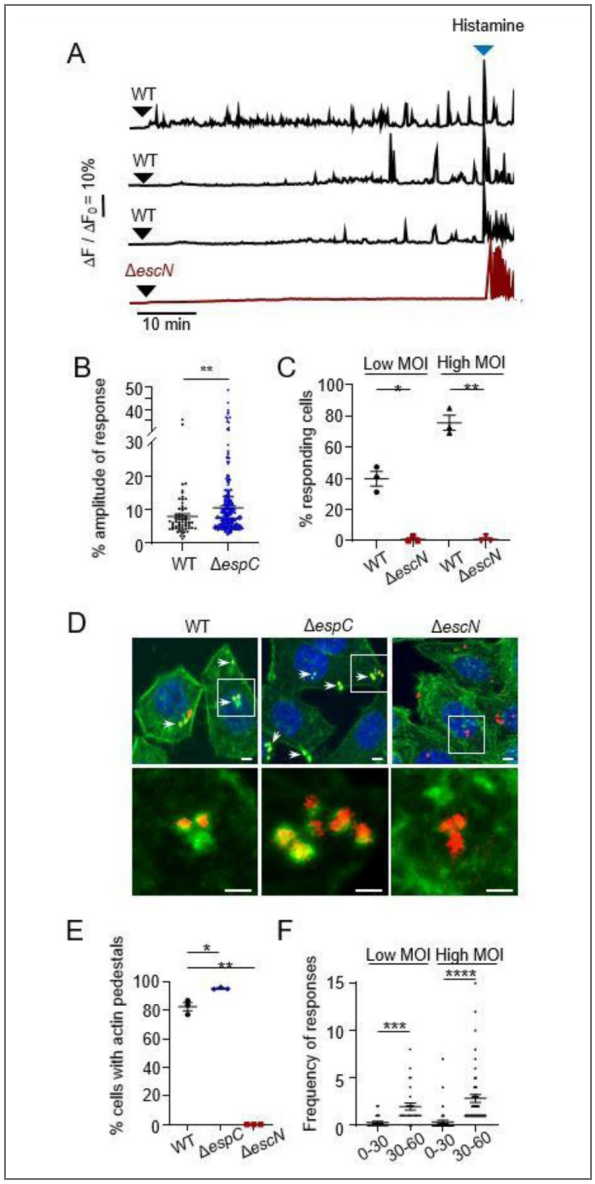


**Figure 1. EPEC induces isolated $Ca^{2+}$ responses of limited amplitude in epithelial cells.**

HeLa cells were loaded with the fluorescent indicator Cal-520, challenged with the indicated bacteria and subjected to live-cell $Ca^{2+}$ imaging at a frequency of one acquisition every 10 seconds (**A-C, F**) or fixed and processed for fluorescence microscopy analysis (**D-E**) (Materials and Methods). **A**, Representative traces of $Ca^{2+}$ variations in single cells. The black arrowheads indicate the time of bacterial challenge. The blue arrowheads indicate stimulation with 3 µM histamine. **B**, Response amplitude expressed as a percent of the maximal histamine response amplitude (N = 3, n > 63). **C**, Percent of cells exhibiting $Ca^{2+}$ responses (N =3, cells > 66). (**D, E**) Cells challenged with RFP-expressing bacteria for 1 hour. **D**, Representative confocal micrographs. Staining with DAPI (blue), phalloidin-Alexa 488 (green). The lower panels show a higher magnification of the insets in the top panels. Scale bar = 10 µm. **E**, Percentage of bacteria-associated actin-rich pedestals (N = 3, cells > 273). **F**, average number of responses per cell during the first 30 min (0-30) and last 30 min (30-60) of bacterial challenge. Low MOI: 10 bacteria / cell. High MOI: 50 bacteria / cell. Bar: mean. (N = 3, cells > 63). Mann-Whitney test. *: $p < 0.05$; **: $p < 0.01$; ***: $p < 0.001$; ****: $p < 0.0001$.

Consistent with this and as shown in Figs. 2A-C, an *espC* mutant induced more $Ca^{2+}$ responses than wild-type EPEC, with 94 ± 3% responding cells and a frequency of 10.5 ± 1.2 responses per cell over the 60 min analysis, compared 40 ± 4.7% responding cells and less than 2 responses per cell for the *espC* mutant and wild-type EPEC, respectively. Also, the average amplitude of $Ca^{2+}$ responses induced by the *espC* mutant was higher than that of wild-type EPEC, suggesting more eATP release (Fig. 1B). Accordingly, cell treatment with the purinergic receptors's antagonists Suramin and PPADS as well as with hexokinase to deplete eATP, inhibited $Ca^{2+}$ responses induced by the wild-type and *espC* mutant strains (Figs. 2B, C, S2A-C). Treatment with the PLC inhibitor U73122, but not its inactive analog U73343, also resulted in inhibition of EPEC-mediated $Ca^{2+}$ responses (Figs. S2A, B). As expected for ATP-mediated $Ca^{2+}$ release, sample treatment with EGTA, a cell impermeant chelator of extracellular $Ca^{2+}$ did not decrease the percent of $Ca^{2+}$ responding cells triggered by wild-type EPEC or the *espC* mutant (Fig. S2C). The frequency of responses per cell was also not inhibited and even appear to increase upon EGTA-treatment in cells challenged with wild-type EPEC and the *espC* mutant (Figs. S2D, E). In control experiments, Suramin treatment did not affect actin pedestal structures induced by these strains (Fig. S3).

Together, these results suggest that $Ca^{2+}$ responses induced by EPEC are mediated by ATP released in the extracellular medium via pores formed by the T3SS translocon and are down-regulated by EspC.

## EPEC induces coordinated $Ca^{2+}$ responses from single $IP_3R$ clusters

We previously showed that *Shigella* induced local $Ca^{2+}$ responses dependent on the T3SS and $Ca^{2+}$ release (Tran Van Nhieu et al., 2013), suggesting that insertion of the Type III translocon was responsible for bacterial-induced local $Ca^{2+}$ signals. We therefore set up to investigate whether EPEC could also trigger T3SS-dependent local $Ca^{2+}$ responses.

To explore this, we performed rapid $Ca^{2+}$ imaging at a frequency of 57 ms acquisition per frame to sample elementary $Ca^{2+}$ release events. As shown in Fig. 3, by performing high speed $Ca^{2+}$ imaging, we detected fast $Ca^{2+}$ increases associated with cell challenge with EPEC. These fast $Ca^{2+}$ responses did not correspond to other responses previously reported since they involved the whole cell or a large cell area but showed a small amplitude and fast dynamics usually associated with local $Ca^{2+}$ responses (Fig. 3B). As observed for the ATP-dependent responses shown in Fig. 2, the *espC* mutant triggered a higher percent of $Ca^{2+}$ responding cells than wild-type EPEC (Fig. 3C). Also, the response amplitude was higher for the *espC* mutant with an average amplitude corresponding to 7.7 ± 0.4 % (mean ± SEM) of the maximal agonist response, compared to 5.4 ± 0.4 % (mean ± SEM) for wild-type EPEC (Fig. 3E). These responses occurred repeatedly at a high frequency of up to 4.5 responses per minute during several minutes following bacterial challenge (Figs. 3D and 3F) and were dependent on Type III Secretion, as evidenced by the lack of response in cells infected with the *ΔescN* strain (Figs. 3B and 3C). EPEC-induced fast $Ca^{2+}$ responses were dependent on $Ca^{2+}$ release since they were inhibited by U73122, a PLC inhibitor (Figs. 3C and 3D). These similarities with the EPEC-induced eATP-dependent $Ca^{2+}$ responses suggested that the atypical fast responses were triggered by low amounts of ATP released in the extracellular medium following insertion in host cell plasma membranes of discrete numbers of EPEC T3SS translocons. Consistently, these atypical EPEC-induced fast responses were abolished in the presence of the ATP receptor inhibitor Suramin (Figs. 3C, D).

Together, these results show that at the onset of infection, EPEC induces an atypical pattern of fast $Ca^{2+}$ responses involving the whole or a large area of the cell, likely resulting from low ATP levels released by the insertion of a discrete number of translocons in host cell membranes.

## EPEC-induced fast $Ca^{2+}$ responses are triggered by low ATP levels

Previous studies have described local $Ca^{2+}$ increases triggered by sub-maximal agonist concentrations and leading to limited $IP_3$-mediated $Ca^{2+}$ release. These local $Ca^{2+}$ responses are typically small, of short durations and localized to subcellular regions. Among these, the so-called "Blips" correspond to elementary events of opening of a single $IP_3$ receptor channel usually lasting

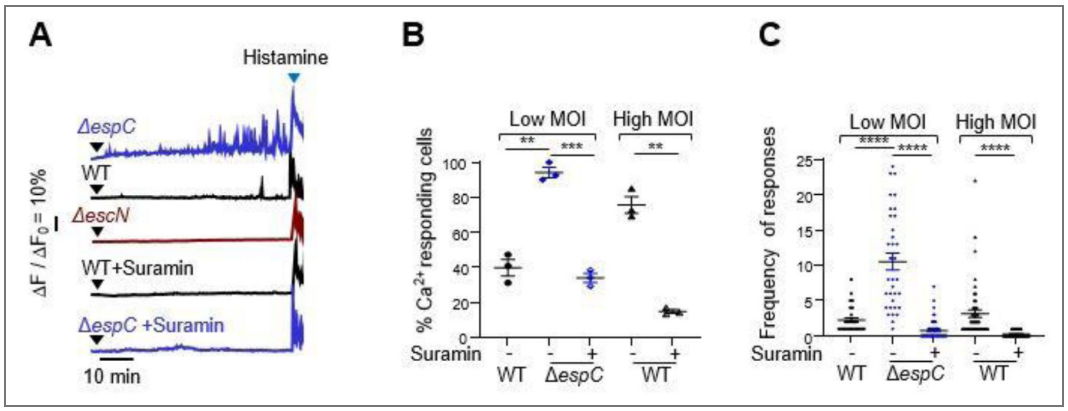


**Figure 2. EPEC-induced $Ca^{2+}$ responses are elicited by ATP released by the T3SS translocon**

HeLa cells were loaded with the fluorescent indicator Cal-520 or with 200 μM suramin for 30 minutes, challenged with the indicated bacteria and subjected to live-cell $Ca^{2+}$ imaging for a 60 min-duration at a frequency of one acquisition every 10 seconds. **A**, Representative traces of $Ca^{2+}$ variations in single cells. The black arrowheads indicate the time of bacterial challenge. The blue arrowheads indicate stimulation with 3 μM histamine. **B**, Percent of cells exhibiting $Ca^{2+}$ responses (N = 3, cells > 70). **C**, Average number of responses per cell. Low MOI: 10 bacteria / cell. High MOI: 50 bacteria / cell. Bar: mean. (N = 3, cells > 30). Mann-Whitney test. **: $p < 0.01$; ***: $p < 0.001$; ****: $p < 0.0001$.

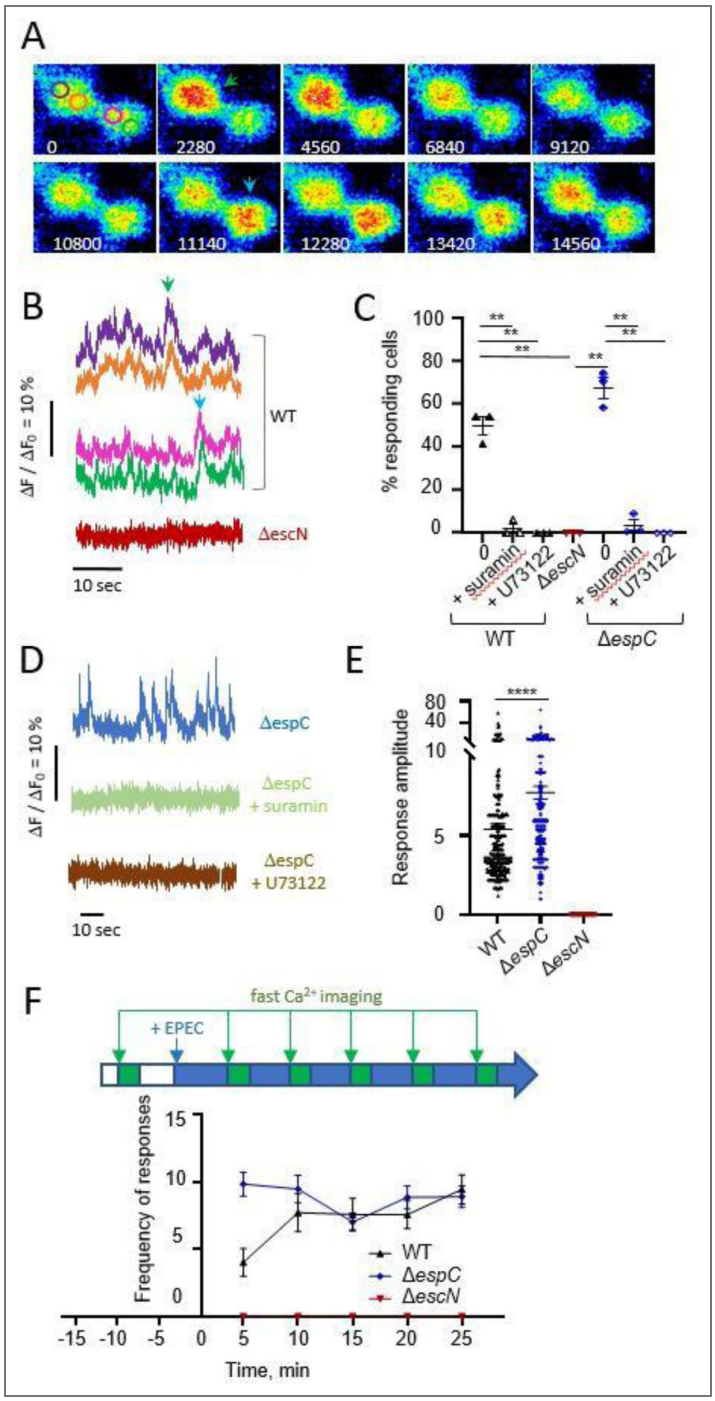


**Figure 3. EPEC induces rapid and Coordinated Elementary $Ca^{2+}$ Responses.**

HeLa cells were loaded with the fluorescent indicator Cal-520, challenged with the indicated bacteria and subjected to high speed $Ca^{2+}$ imaging at a frequency of one acquisition every 57 ms for a duration of 110 seconds. **A**, Representative time-serie of pseudocolored fluorescent micrographs of cells challenged with wild-type EPEC. The numbers indicate the elapsed time in ms from an arbitrarily determined origin. Scale bar = 10 µm. **B**, **D**, traces of $Ca^{2+}$ variations in 2 subcellular regions of the same cell. **B**, WT: traces corresponding to the regions depicted in the image 0 of panel **A**. The arrowheads point to the $Ca^{2+}$ responses shown in Panel A with the corresponding color. **C**, Percent of cells exhibiting $Ca^{2+}$ responses (N > 3, cells > 134). + Suramin: treatment with 200 µM Suramin. +U73122: treatment with 10 µM U73122. **E**, Response amplitude expressed as a percent of the maximal response amplitude induced by treatment with 3 µM histamine (N = 3, cells > 166). **F**, average number of responses per cell. **C**, **E**, Bar: mean. Mann-Whitney test. **: $p < 0.01$; ****: $p < 0.0001$. **F**, High speed $Ca^{2+}$ imaging was performed every 5 min for 110 seconds following infection with the indicated bacterial strain as depicted the scheme. The average number of responses per cell is indicated (N > 3, cells > 29).

between 50 and 100 ms, whereas "Puffs" involve the synchronized activation of multiple $IP_3$ receptor channels in localized clusters and last several hundreds of ms (Swillens et al., 1999). In contrast to these described local $Ca^{2+}$ signals, EPEC-induced fast and small responses could occur throughout the cell, suggesting the coordination of elementary responses over large cell area. Since our findings suggested that these responses were elicited by low amounts of eATP released by a discrete number of T3SS translocons, we investigated whether low ATP levels could elicit similar responses.

HeLa cells treated with 150 nM ATP showed $Ca^{2+}$ responses that were indistinguishable from fast responses elicited by EPEC, with an average percent of $Ca^{2+}$ responding cells of 61.2 ± 5.8 % (mean ± SEM) and a frequency of 3.9 responses per cell over 60 seconds (Figs. 4A, C and S4A). These fast $Ca^{2+}$ responses had an amplitude that did not exceed 10 % of the maximal agonist response and occurred over several minutes (Fig. 4A), with a duration of 2.1 ± 1.0 sec (mean ± SEM) (N = 4, 128 responses). As observed for EPEC, fast $Ca^{2+}$ responses induced by low ATP levels involved the whole cell or large cell area encompassing the nuclear and perinuclear area and corresponding to at least 30 % of the cell area as illustrated in Fig. 4B. In this large area, all ROIs corresponding to 1 square micron showed a superimposable profile, as illustrated by traces in Fig. 4C. Similar fast and small coordinated $Ca^{2+}$ responses were also observed when cells were challenged with 100 nM of histamine, another $Ca^{2+}$ agonist, with 44 ± 7 % (mean ± SEM) of cells showing responses, suggesting that these are generic responses triggered by low levels of $IP_3$ (N = 2, cells = 340; Fig. S4). EPEC and low concentrations of eATP induced similar responses in polarized intestinal epithelial cells (Fig. S5).

More detailed scrutinizing showed that in their initial mounting phase, these fast $Ca^{2+}$ responses were created by the opening of discrete clusters involving an area of ca. 0.04 $\mu m^2$ that had a transient activity, or possibly were highly mobile, since they were seldom detected at a similar location for three consecutive 22 ms acquisition frames (Figs. S6A, B). These discrete clusters showed similar $Ca^{2+}$ kinetics suggesting the coordination of $Ca^{2+}$ release of single $IP_3R$ clusters throughout the area that we will hereafter termed CCRICs for "Coordinated $Ca^{2+}$ Responses from $IP_3R$ Clusters". Treatment with BAPTA-AM to chelate intracellular $Ca^{2+}$ led to a complete inhibition of CCRICs (N = 3, n > 150 cells; Fig. S7A). $Ca^{2+}$ responses could still be detected upon cell treatment with EGTA-AM consistent with its lower $k_{on}$ rate for $Ca^{2+}$, but with a significant inhibition of the percentage of $Ca^{2+}$ responding cells as well as of the frequency of responses per cell, suggesting that coordination could occur via $Ca^{2+}$ diffusion and $Ca^{2+}$-induced $Ca^{2+}$ release (Fig. S7).

In rare instances (less than 3%), typical local "Puff" responses elicited by these ATP concentrations could also be detected often occurring at the cell periphery (Figs. 4B, red region and 4C, red arrow; Fig. S6D, blue trace) (N > 20, cells > 500). As expected from the small concentrations of $Ca^{2+}$ released at puff sites, no increase in cytosolic $Ca^{2+}$ was detected in a distal cell region (Fig. S6D, top), indicating that isotropic $Ca^{2+}$ diffusion from a puff release site cannot account for $Ca^{2+}$ increase over large cell area. Puffs could also be detected concomitantly with CCRICs in different ROIs of the same cell (Fig. S6D, bottom). In contrast to puffs, CCRICs often showed responses of comparable amplitude in distal regions over the whole cell (Figs. 4C and S6A, B), suggesting the contribution from $IP_3R$ cluster activation by $Ca^{2+}$-Induced $Ca^{2+}$ Release (CICR). Within a given cell, the vast majority of CCRICs appeared quasi-synchronized at the fatest acquisition rate of 22 ms / frame that we could achieve. However, in few instances a delay could be detected in the elicitation of a peak in distant region of a cell (Fig. S6C). These observations suggest that the quasi-synchronization of CCRICs result from the fast diffusion of $Ca^{2+}$ leading to the activation of $IP_3R$ clusters over large cell area, which may be delayed in a some instances. Scrutinizing of CCRICs showed that while their profiles were comparable, the amplitude of these responses varied in different regions of the cell, with often a single 1 $\mu m^2$ region, likely corresponding the initial firing cluster, showing a prominent amplitude and other regions with smaller amplitude for a given response (Figs. 4B and 4C). For example, in Fig. 4C, the highest amplitude is observed in the red region for peaks 1 and 3, whereas it is observed and in

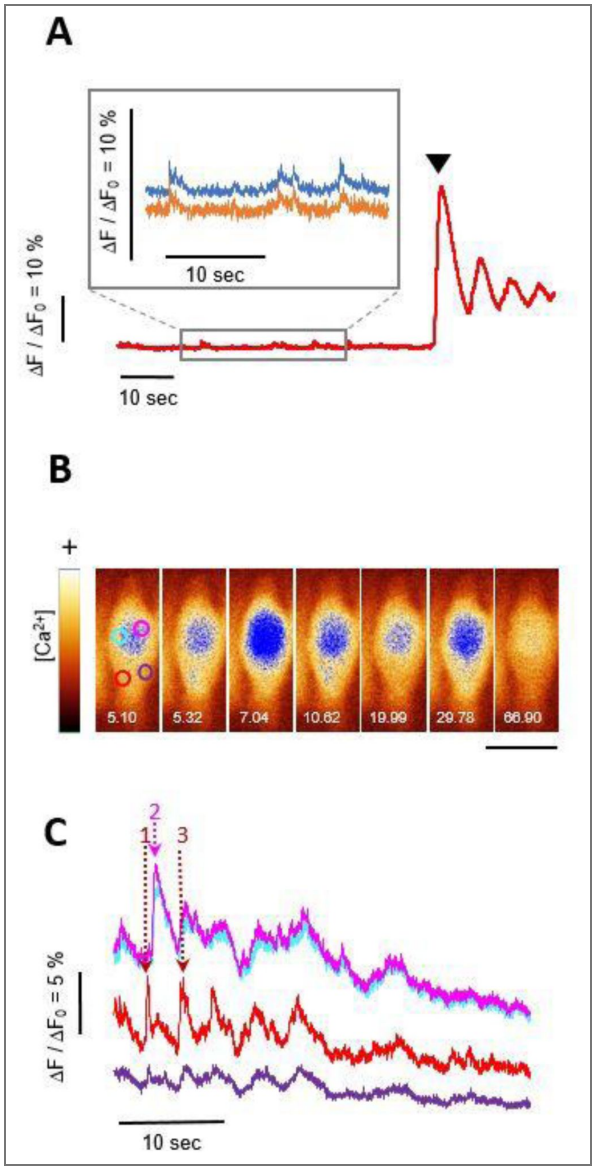


**Fig. 4. EPEC-induced Coordinated Elementary $Ca^{2+}$ Responses are reproduced by low ATP levels.**

**A-C**, HeLa cells were loaded with the fluorescent indicator Cal-520, challenged with 150 nM ATP and subjected to $Ca^{2+}$ imaging. Image acquisition every 52 ms (**A**) or 22 ms (**B**, **C**). **A**, Traces of $Ca^{2+}$ variations corresponding to a single cell (red trace), or subcellular regions within the same cell (inset). **A**, arrowhead: challenge with 2 µM ATP. **B**, Time serie of fluorescent micrographs pseudocolored using the "glow" Fiji lookup table, where the blue pixel correspond to an arbitrarily set threshold value. The numbers indicate the elapsed time in seconds. Blue: high intensity pixels showing the large top cell area with CCRICs and the local lower puff area. Scale bar = 10 µm. **C**, Traces corresponding to $Ca^{2+}$ variations in the subcellular regions depicted in Panel **B**. The responses are labelled 1-4, with the response 1 corresponding to the puff (Panel **B**, red ROI) impulsing the response 3 in the same region. Responses 2 and 4 correspond to CCRICs in Panel **B**, blue and green ROIs. Note the diffusion of the responses from the initial release area in other area inferred from the dampening of the response amplitude.

the purple region for peak 2. Thus, for a given CCRIC, the respective contribution of local $IP_3R$ cluster activation and isotropic diffusion of $Ca^{2+}$from other release sites in $Ca^{2+}$ increase may vary in different regions of the cell.

## CCRICs are coordinated by the rapid diffusion of $Ca^{2+}$ at low concentrations in cell area with a high density of $IP_3$ clusters

In Fig. 5, we used modeling to further investigate the mechanism of coordination of these fast $Ca^{2+}$ responses. Based on our previous studies (Voorsluijs et al., 2019; Ornelas-Guevara et al., 2023), the model provides a fully stochastic spatial description of $Ca^{2+}$ release dynamics from $IP_3R$ clusters in a two-dimensional representation of a HeLa cell. The simulation domain extends on 10 × 10 $\mu m^2$ and is discretized into a 20 × 20 grid of compartments (0.5 × 0.5 $\mu m^2$ each), each representing a cytosolic subvolume of $10^{-16}$ L. Each compartment contains at most one cluster of $IP_3R$, whose dynamics is described as a whole. Besides, cytosolic $Ca^{2+}$ concentration can also vary because of uptake by SERCA, release by a leak or diffusion (Supplementary Information, Note 1).

In Fig. 5A, low ATP levels lead to low $IP_3$ levels activating a limited number of $IP_3$ clusters, opening stochastically and releasing small amounts of $Ca^{2+}$. In a given area of the cell, the $Ca^{2+}$ variation integrates $Ca^{2+}$ release from clusters within this area, as well as $Ca^{2+}$ diffusing from or to other cell area. For a given response, the initially firing cluster is contained in an area characterized by the highest $Ca^{2+}$ peak amplitude (Fig. 5A, blue and green arrows) that dampens in a distal area (Fig. 5A, blue and green arrowheads). If the density of $IP_3R$ clusters is low, as expected for ER compartment at the cell periphery, the spatial segregation of the initial firing cluster and resulting $Ca^{2+}$ diffusion to other area is clearly detected (Fig. 5A). In instances, however, the model predicts temporally coordinated responses of similar amplitude, suggesting $Ca^{2+}$-induced $Ca^{2+}$ release from secondary clusters (Fig. 5A, black arrow). For both type of $Ca^{2+}$ dynamics, a large value of the $Ca^{2+}$ diffusion coefficient of 100 $\mu m^2$ / s is a key parameter that needs to be taken into account in the model. While it is generally admitted that $Ca^{2+}$ diffuses very slowly due to the $Ca^{2+}$ buffers in the cell (~30 $\mu m^2$/s), the low levels of $Ca^{2+}$ released by CCRICs may not be subjected to the diffusion limitations observed at higher $Ca^{2+}$ levels, because of the relative moderate affinity of buffers for $Ca^{2+}$. How the effective diffusion coefficient of $Ca^{2+}$ is affected by the $Ca^{2+}$ concentration is explained in more detail in Supplementary Information, Note 2.

If the $IP_3R$ cluster density is high, as expected in the large perinuclear and nuclear area corresponding to the bulk of the ER, the coordination between individual clusters is very fast (Fig. 5B). As a result, the identification of initial firing clusters goes beyond the technical capacities of the imaging set-up, and ROI within this area show comparable profiles of fast $Ca^{2+}$ responses (Fig. 5B). Upon prolonged incubation with increasing $Ca^{2+}$ responses and sensitization of $IP_3R$ clusters, the coordination of responses linked to $Ca^{2+}$-induced $Ca^{2+}$ release becomes predominant throughout the cell (Fig. 5C). Moreover, at high $IP_3$ concentrations, the model reproduces the propagation of a large-amplitude $Ca^{2+}$ wave, as expected (Supplementary Information, Note 3).

## Low eATP levels dampen NF-κB activation

Our findings indicate that the novel $Ca^{2+}$ response pattern is not exclusive to EPEC infection and can be replicated by low levels of eATP or histamine, suggesting a broader physiological relevance. From an immunological perspective, CCRICs may therefore play a critical role in various signaling pathways during bacterial infection. eATP is a well-characterized danger signal contributing to the elicitation of pro-inflammatory signals in various tissues in response to infections (Savio et al., 2018). Previous studies linked intracellular $Ca^{2+}$ signaling and NF-κB activation, a key transcription factor that triggers inflammatory responses (Smedler et al., 2014). We therefore set up to investigate the effects of CCRICs triggered by low eATP levels on NF-κB activation, by performing Western blot analysis against the phosphorylated forms of IκBα (p- IκBα) and P65 (p-P65).

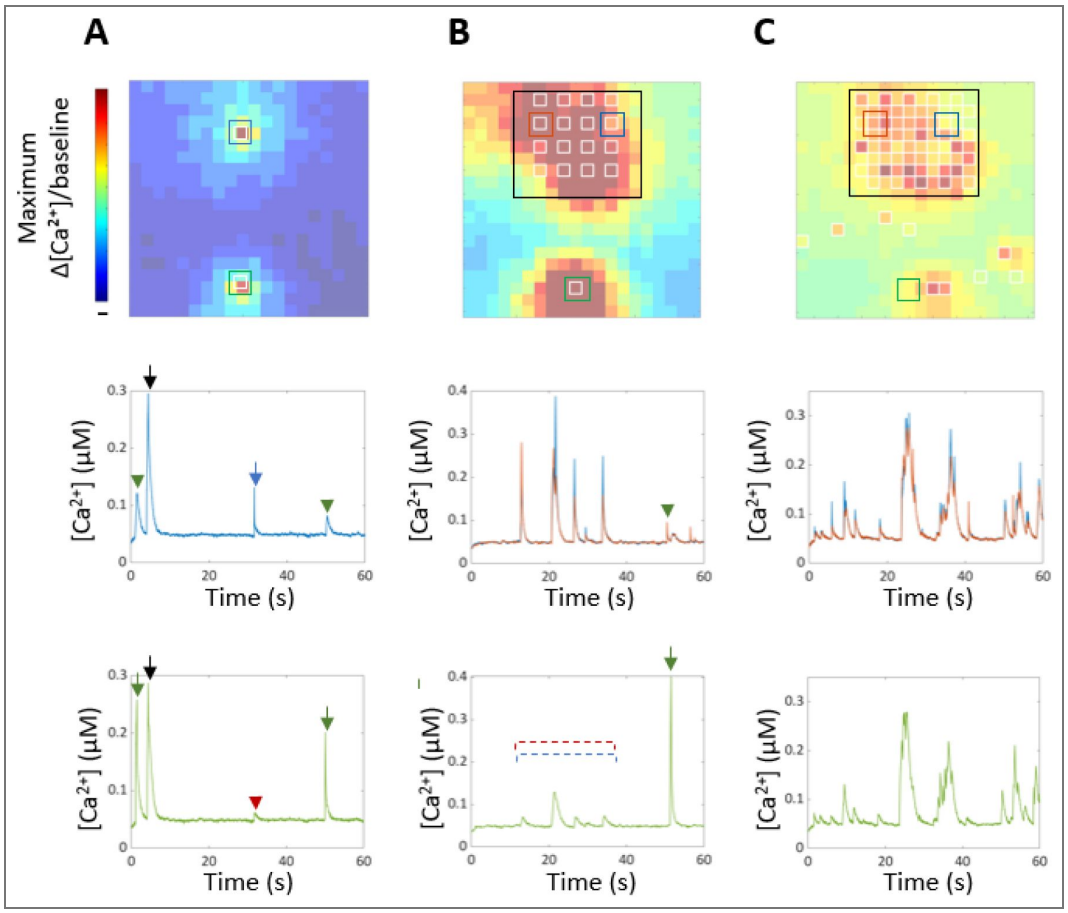


**Fig. 5. Modeling of Coordinated Elementary $Ca^{2+}$ Responses.**

**Top**, $Ca^{2+}$ variations in subcellular area within a single cell are represented in pseudocolor. Shown are the maximum values of $\Delta[Ca^{2+}]/[Ca^{2+}]_b$ reached in each compartment during a 60s simulation. Empty white squares: $IP_3R$ clusters. **Graphs**, Traces correspond to $Ca^{2+}$ variations in the region with the matching color. Colored arrows: $Ca^{2+}$ response due to the activation of an $IP_3$ cluster in the region with the matching color. Colored arrowhead and dashed red and blue lanes: $Ca^{2+}$ variations due to the diffusion of a $Ca^{2+}$ response from or nearby to the region with the matching color. Black arrows: $Ca^{2+}$ response due $Ca^{2+}$-activated $Ca^{2+}$ release. **A**, low density of $IP_3R$ clusters with local responses detected. **B**, **C**, Empty black box: area with a high density $IP_3R$ clusters. **C**, similar to **B**, but following $IP_3R$ cluster sensitization due to increased $Ca^{2+}$ responses.

As shown in Figs. 6A and 6B, in control samples, TNF-α induced IκB-α phosphorylation peaking 10 minutes following challenge. In contrast, in the presence of low ATP levels, IκB-α showed a delayed phosphorylation with a 2.1 fold decrease at 10 minutes post-challenge (Figs. 6A and 6B). Consistently, the rates of IκB-α degradation were also slower in the presence of ATP relative to control (Figs. 6A and 6C). As expected from the IκB-α results, TNF-α induced the phosphorylation of the NF-κB P65 subunit and ATP led to a delay and decrease in P65 phosphorylation (Figs. 6D and 6E).

In control experiments, we did not detect differences in P65 phosphorylation in response to TNF-α stimulation when cells were treated with BAPTA-AM to chelate intracellular $Ca^{2+}$ (Figs. 6F and 6H). However, cell treatment with BAPTA-AM prevented the dampening of P65 phosphorylation triggered by low ATP levels (Figs. 6G and 6H), suggesting that CCRICs down-regulated TNF-α -induced NF-κB activation.

## Low eATP levels down-regulates NF-κB activation through $Ca^{2+}$-dependent O-GlcAcylation

We next investigated how CCRICs could regulate NF-κB activation. O-linked β-N-acetylglucosamine (O-GlcNAc) transferase (OGT) was reported to regulate NF-κB signaling by post-translationally modifying the p65 subunit (Ruan et al., 2017). Interestingly, OGT is regulated by $Ca^{2+}$ signaling, suggesting that CCRICs could affect NF-κB activation via O-GlcNAcylation.

As shown in Fig. S6, TNF-α in the presence of 150 nM eATP stimulated the levels of O-GlcNacylation, specifically for proteins with an apparent molecular weight superior to 100 kDa that was not observed with TNF-α alone. To further investigate the effects of low eATP levels on NF-κB O-GlcNacylation, we performed immunoprecipitation of P65 RelA on lysates of cells stimulated for 12 minutes with TNF-α alone or co-stimulated with TNF-α and 150 nM eATP. As shown in Fig. 7, TNF-α induced increased O-GlcNacylation of P65 relative to non-stimulated cells, but this increase was inhibited by low eATP levels. Inhibition of P65 O-GlcNacylation by eATP was $Ca^{2+}$ dependent, since it was not observed in the presence of BAPTA-AM (Fig. 7).

The results indicate that low eATP levels inhibit O-GlcNacylation of P65 induced by TNF-α in a $Ca^{2+}$-dependent manner and suggest that differential O-GlcNacylation of P65 relative to higher molecular weight proteins.

# Discussion

We report here the characterization of CCRICs, corresponding to yet undescribed $Ca^{2+}$ responses. CCRICs showed rapid kinetics with an average duration of ca 2.1 seconds and amplitude corresponding to an increase in $Ca^{2+}$ cytosolic concentration of a few hundreds nM, seemingly smaller than that of puffs (Fig. S6D), often occurring repeatedly with a frequency of up to 12 CCRICs / min over the whole cell. Our modelling studies support the notion that CCRICs implicate the rapid coordination of $IP_3R$ clusters via CICR in large cell area, challenging established concepts in the $Ca^{2+}$ signaling field.

$Ca^{2+}$ diffusion in the cytosol is regulated by mobile and immobile $Ca^{2+}$-binding proteins acting as buffers and forming localized microdomains with steep $Ca^{2+}$ concentration gradients. At the mouth of an open $IP_3R$ channel, $Ca^{2+}$ concentration can reach 100 μM, while just 1–2 μm away, it may drop below 1 μM. Diffusion is restricted by $Ca^{2+}$ buffers with $K_D$'s that are generally lower than this concentration. Consequently, $Ca^{2+}$ signaling is generally admitted to be spatially restricted, typically influencing regions within approximately 5 μm of the release site (Foskett et al., 2007). The distribution of $Ca^{2+}$-binding proteins and the spatial arrangement of release channels allow $IP_3R$-mediated $[Ca^{2+}]_i$ signals to exhibit diverse spatial and temporal properties, making this system highly adaptable (Vandeput et al., 2007). High-resolution optical imaging of fluorescent $Ca^{2+}$ indicators in intact cells indicates that $IP_3$-mediated $[Ca^{2+}]_i$ signals are structured levels (Foskett et al., 2007). At low $IP_3$ levels, individual $IP_3R$ opens stochastically at discrete release sites, causing localized elevations in cytoplasmic $[Ca^{2+}]$. At higher $IP_3$ levels, $Ca^{2+}$ release spreads between $IP_3R$ clusters, propagating waves that travel at tens of microns per second,

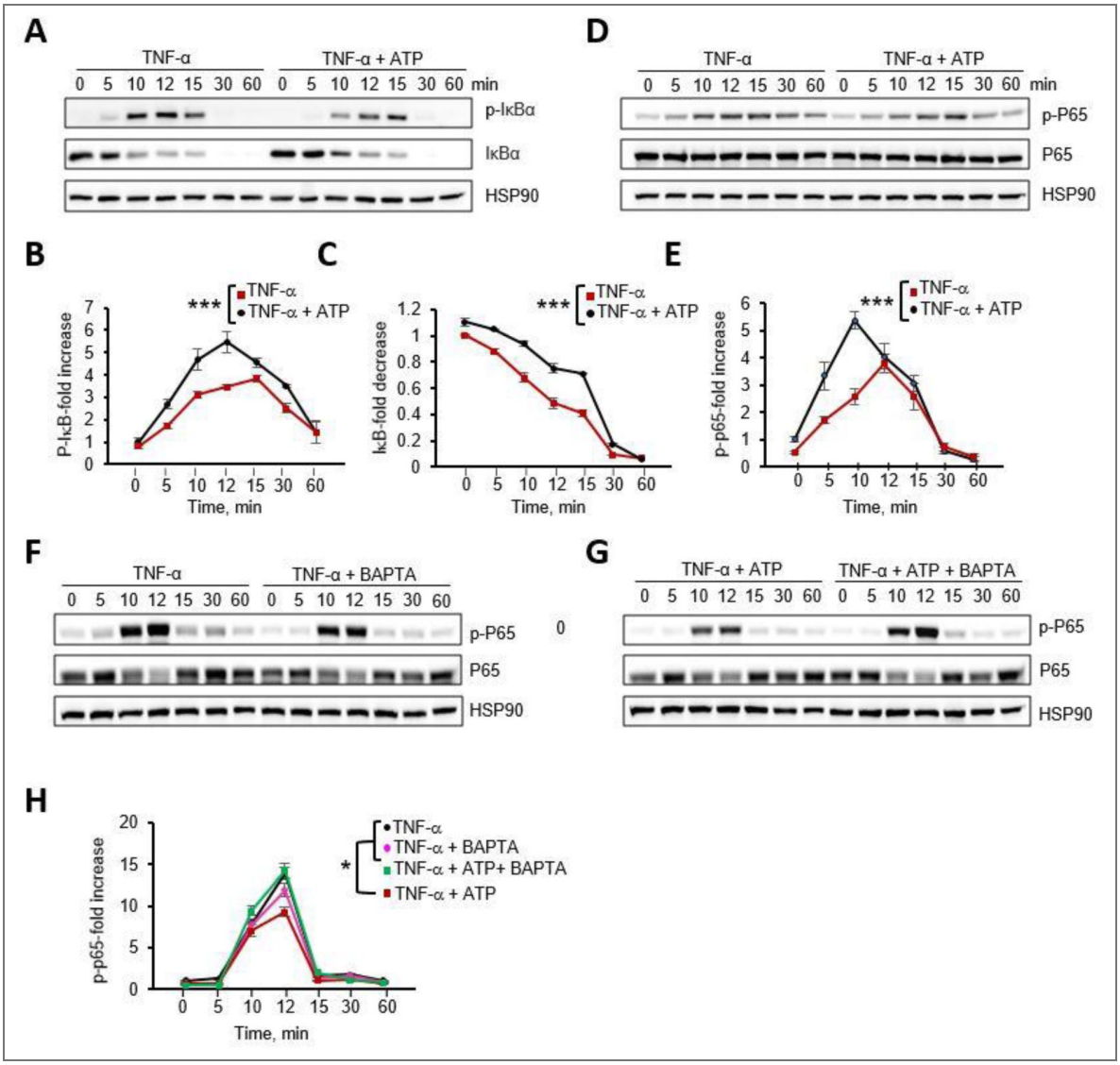


**Fig. 6. Low ATP levels dampen NF-kappaB activation.**

HeLa cells were stimulated with 10 ng/ml TNF-α alone or in the presence of 150 nM ATP or 20 μM BAPTA-AM (**F**-**H**). At the indicated time points, cell lysates were analyzed by Western blot using the indicated antibodies**. A**, **D**, **F**, **G**, Representative blots. **B, C, E**, **H**, Densitometry analysis of the indicated antibody signal normalized to that of HSP90 (**B, C**) or total P65 (**E, H**), expressed as fold-increase to basal levels of p-IκB (**B**), IκB (**C**) or p-p65 (**E**, **H**) at time = 0. Values correspond to the mean ± SEM of 3 or 4 independent experiments. p-p65: anti-phospho P65 antibody. p-IκB: anti-phospho IκB antibody. ANCOVA test. *: $p < 0.05$; **: $p < 0.01$; ***: $p < 0.001$.

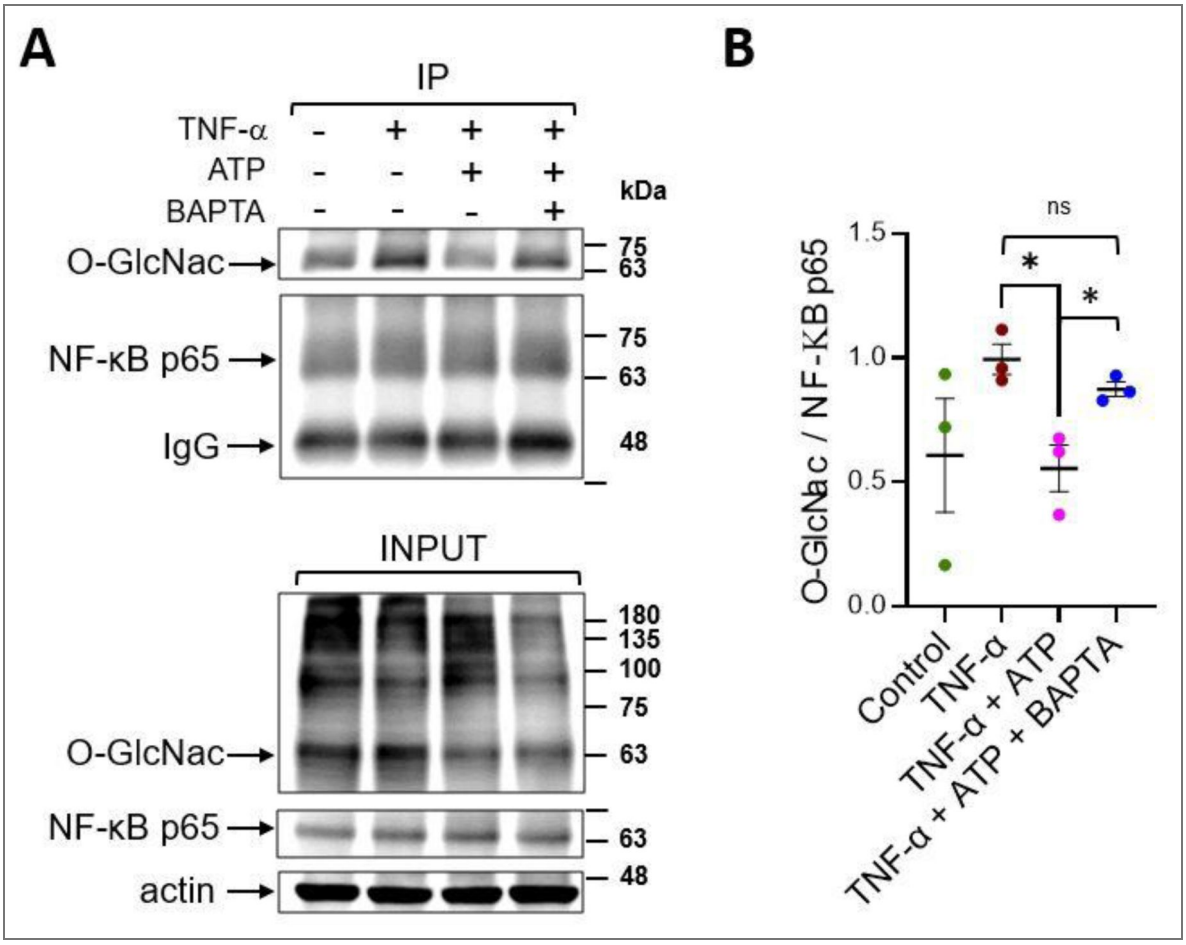


**Fig. 7. Low ATP levels down-regulate NF-kB O-GlcNAcylation in a $Ca^{2+}$-dependent manner.**

HeLa cells were stimulated with 10 ng/ml TNF-α alone or in the presence of 150 nM ATP with or without 20 μM BAPTA-AM for 12 min. Cell lysates were subjected to P65 immunoprecipitation. **A**, Representative blots with the indicated antibodies. IP: immunoprecipitates; L: total cell lysates. **B**, Densitometry analysis of the O-GlucNAc signal in P65 immunoprecipitates normalized to that of TNF-α alone. Mann-Whitney test. N = 4. *: $p < 0.05$. ns: not significant.

coordinating intracellular signaling ultimately leading to a global $Ca^{2+}$ response. In reference models describing intracellular $Ca^{2+}$ dynamics, cell regions with a high $IP_3R$ density initiate the $Ca^{2+}$ response from which $Ca^{2+}$ waves propagate with a diffusion coefficient of 10 – 30 $\mu m^2/s$ (Falcke et al., 2003).

In contrast to these described global and local $Ca^{2+}$ responses, we found CCRICs to be highly temporally coordinated over large area, suggesting the fast diffusion of $Ca^{2+}$ and propagation of $Ca^{2+}$ by CICR. While challenging generally admitted concepts on the poor diffusion of $Ca^{2+}$, this view is fully supported by our theoretical modeling implicating the fast diffusion of $Ca^{2+}$, with a diffusion coefficient of at least 100 $\mu m^2/s$ that can be expected at low cytoplasmic [$Ca^{2+}$]. Indeed, at these low $Ca^{2+}$ concentrations not exceeding a few hundreds nM, the majority of $Ca^{2+}$ buffers are not expected to efficiently bind to $Ca^{2+}$ and to significantly interfere with $Ca^{2+}$ diffusion because of their relative low affinity.

We found that CCRICs implicate a large cell area including the nuclear and perinuclear area. The large CCRIC area likely involves the bulk of the endoplasmic reticulum, while peripheral area may contain smaller ER compartments. In our model considering fast $Ca^{2+}$ diffusion when buffers are far from saturation, the higher density of $IP_3R$ clusters in the CCRIC area accounts for the high coordination of the responses, relative to the lack of coordination in peripheral area where lower $IP_3R$ density is expected. Consistently, while CRICCs were detected in the vast majority of cells at these very low agonist concentrations, in rare instances, local “puff-like” responses were also detected at the cell periphery. These observations are in contrast to previously described $Ca^{2+}$ puffs preceding global responses reported to occur preferentially in perinuclear area (Thomas et aL., 1999). These earlier studies, however, involved higher agonist concentrations (1-5 µM ATP) expected to lead to the release of higher $IP_3$ concentrations, which may preferentially stimulate larger $IP_3R$ clusters at the perinuclear region because of the higher density of $IP_3Rs$. In addition, larger $IP_3$ clusters may release higher amounts of $Ca^{2+}$ for which, as opposed to CCRICs, diffusion would be restrained by $Ca^{2+}$ buffers thereby favoring the spatial confinement of the response.

We showed that a low dose of eATP triggering CCRICs delayed and dampened NF-κB activation linked to a reduction in O-GlcNAcylation of the NF-κB p65 subunit. One major open question is the mechanism by which CCRICS down-regulate NF-κB activation. NF-κB activity can be modulated by O-GlcNAcylation, a reversible glycosylation modification catalyzed by O-GlcNAc transferase (OGT) and O-GlcNAcase (OGA) (Liu & Ramakrishnan, 2021). Previous studies demonstrated that $Ca^{2+}$ signals activate $Ca^{2+}$-regulated enzymes like CaMKII, which in turn phosphorylates and activate OGT, promotes O-GlcNAcylation (Ruan et al., 2017). In other studies, OGT-mediated O-GlcNAcylation could modulate NF-κB signaling pathway (X. Dong et al., 2023). O-GlcNAcylation of P65 could also inhibit its interaction with IκB-α, promote p65 nuclear translocation and increase NF-κB transcriptional activity (Liu & Ramakrishnan, 2021). Reduced O-GlcNAcylation of P65 at residues S550 and S551 was shown to result in decreased NF-κB activation and nuclear translocation (Motolani et al., 2023). These findings are in line with our results suggesting that CCRICs elicited by low-level eATP, downregulate p65 O-GlcNAcylation and NF-κB activation, possibly by modulating OGT activity or OGT-p65 interactions. Reduced O-GlcNAcylation of p65 may affect its phosphorylation patterns indirectly, perhaps by altering the interaction of NF-κB with kinases or phosphatases involved in its activation (Özcan et al., 2010).

Our findings indicate that eATP differentially regulate inflammatory signaling pathways in epithelial cells by dampening NF-κB activation at low levels and stimulating its activation at high concentrations. These results extend the key role of eATP from a danger-associated molecular pattern (DAMP) to a fine-tuner of inflammatory responses depending on its concentration.

# Materials and Methods

## Cell and Bacterial culture

HeLa cells were maintained in Dulbecco’s Modified Eagle Medium (DMEM; Gibco, Thermo Fisher Scientific) supplemented with 10% fetal bovine serum (FBS; Gibco, Thermo Fisher Scientific) Human colon adenocarcinoma Caco-2/TC-7 cells were maintained in DMEM containing 20 % FBS,

supplemented with non-essential amino acids. Cells were grown at 37 °C in a humidified incubator with 10% $CO_2$. Wild-type Enteropathogenic Escherichia coli (EPEC WT), *ΔescN*, and *ΔespC* strains were cultured in Luria-Bertani (LB) broth at 37 °C with kanamycin at a final concentration of 15 μg/ml in a shaking incubator. All strains were transformed with the pmCherry-N1 plasmid, which encodes red fluorescent protein and carries an ampicillin resistance gene for selection. Where applicable, ampicillin (100 μg/mL) and kanamycin were included to maintain resistance markers. The red fluorescence enabled visualization of the bacteria during downstream analyses.

## EPEC infection of cells

HeLa cells were seeded in 6-well plates at a density of $4.5 \times 10^5$ cells per well one day before infection. TC-7 cells were seeded at a density of $5 \times 10^5$ cells / well in 6-well plates and allow to polarize for 4 days prior to bacterial challenge, replacing medium every day. EPEC WT, *ΔescN*, and *ΔespC* strains grown in the exponential phase were resuspended and primed for 5 hours before challenging HeLa cells in DMEM medium. Cells were challenged with bacteria at an OD600 = 0.2 (Low MOI) or 0.8 (High MOI).

## $Ca^{2+}$ imaging

HeLa cells were seeded onto 25 mm-diameter glass coverslips. Cells were preloaded with the fluorescent indicator dye Cal-520 (AAT #21130) for 30 minutes at room temperature, followed by two PBS washes and one time with DMEM. And placed coverslips, imaging was performed in an observation chamber in DMEM without phenol red, supplemented with 25 mM HEPES. Following a 3-minute baseline acquisition, add the required bacteria strains and OD600 into the chamber. Following a 10-minute incubation at room temperature to allow bacterial attachment. Imaging was then carried out at 35°C to allow for bacterial type III secretion, using a Nikon Eclipse TE200 inverted fluorescence microscope with a 60× objective for 1h of infection. Fluorescence signals were acquired 485 nm with excitation and 535 nm emission parameters. Image control and data acquisition were managed by Simple32 software (Compix Inc.), depending on the experiment requirement, imaging at 22ms, 57ms or 10 sec acquisition intervals. 3 μM of Histamine and 2 μM of ionomycin were applied to check the ability of cells to show calcium response. Images were captured using a CMOS camera (Hamamatsu) and analyzed using the same software.

## Immunofluorescence analysis

Cells were washed three times with PBS and fixed with 3.7% paraformaldehyde (PFA), permeabilized with 0.1% Triton X-100 for 5 minutes and washed with PBS. Blocking was performed using 3% FBS in PBS for 30 minutes at room temperature. Cells were incubated with anti-Z0-1 polyclonal antibody (ThermoFisher Scientific, # 40-2200) for 1 hour at a 1:50 dilution in PBS containing 1% FBS for an hour, followed by anti-rabbit IgG-Alexa 488 (Life Technologies, #A11034) or mouse phalloidin-Alexa 488 (Fischer Scientific, #17511176) at a 1:200 dilution and DAPI (1 μg/ml; Merck, #102362276001) for another hour. Samples were mounted using Dako mounting medium (Agilent) and imaged using a Nikon Ti2 confocal microscope equipped with a 60× objective and Nikon acquisition software.

## Modelling

We develop a fully stochastic spatial model to simulate $Ca^{2+}$ release dynamics from $IP_3R$ clusters in a two-dimensional representation of a HeLa cell. The simulation domain measures $10 \times 10$ $\mu m^2$ and is discretized into a $20 \times 20$ grid of compartments ($0.5 \times 0.5$ $\mu m^2$ each), each representing a cytosolic subvolume of $10^{-16}$ L. $Ca^{2+}$ exchange between the Endoplasmic Reticulum (ER) and the cytosol occurs through $IP_3R$-mediated release, SERCA uptake, and ER $Ca^{2+}$ leak, following the framework by Voorsluijs et al., 2019 and Ornelas-Guevara et al., 2023. $Ca^{2+}$ diffusion is implemented stochastically as a kinetic process between adjacent compartments (Kraus et al., 1996), with a diffusion coefficient of 100 $\mu m^2/s$ to reflect moderate endogenous buffering. Each $IP_3R$ cluster functions as a single unit with four possible states: Open (O), Closed (C) and two

Inhibited states (i1, and i2), transitioning in response to local [$Ca^{2+}$] and [$IP_3$]. This phenomenological description captures key characteristics of $Ca^{2+}$ puffs and their transition to global signals via $Ca^{2+}$ diffusion and Calcium Induced Calcium Release.

We perform all simulations using the Gillespie algorithm, where each event, reaction or diffusion, is selected stochastically based on its propensity. See Supplementary Information S1 for additional information about the model.

## Western Blot analysis

To obtain total cell extracts, cells were lysed in sample buffer 1x (62.5 mM Tris pH=8, 2% SDS, 10% glycerol, 0.05% bromophenol blue, 5% β- mercaptoethanol) and boiled at 95°C for 5 minutes. Proteins from total lysates were separated by SDS PAGE and transferred to nitrocellulose membrane (0.45μM AmershamTM ProtranTM). Western Blot analysis was performed according to standard procedure using the following primary antibodies diluted in PBS containing 0.1 % Tween-20 and 5 % non-fat milk: IκB-alpha (OZYME, #9424S) at a 1:1000 dilution, Phospho-IκB-α (OZYME, #9424S) at a 1:1000 dilution, NF-κaB p65 (OZYME, #9246S) at a 1:5000 dilution, Phospho-NF-κB p65 (OZYME, #3033S) at a 1:1000 dilution, HSP90 (Santa Cruz Biotechnologies #sc-13119) at a 1:1000 dilution. The secondary HRP-conjugated anti-mouse (Cytiva) and anti-rabbit (Sigma) antibodies were used at a $10^{-4}$ dilution.

## Immunoprecipitation assays

HeLa cells were seeded in 150 $cm^2$ dishes ($7.4 \times 10^6$ cells/dish) and cultured in DMEM supplemented with 10% FBS. Cells were pretreated with 20 μM BAPTA for 30 minutes at room temperature where indicated, then stimulated with 10 ng/mL TNF-α alone or in combination with 150 nM ATP for an additional 12 minutes. After treatment, cells were washed with ice-cold PBS containing 1 mM NaF and 1 mM $Na_3VO_4$, lysed in ice-cold lysis buffer (50 mM Tris-HCl pH 7.5, 0.5% Triton X-100, 100 mM NaCl, 1 mM DTT, protease inhibitor cocktail without EDTA), and incubated on a rotating wheel at 4°C for 1 hour. Lysates were clarified by centrifugation at 13,000 rpm for 30 minutes at 4°C. Supernatants were incubated with 5 μL of anti-NF-kB p65 antibody (Abcam, ab16502) for 2 hours at 4°C with rotation, followed by overnight incubation with pre-equilibrated protein A/G beads. Immunocomplexes were washed once with lysis buffer and twice with PBS, then eluted in Laemmli buffer by boiling at 100°C for 5 minutes. Input and IP samples were analyzed by Western blotting using antibodies against O-GlcNAc (Abcam, ab2739), anti-NF-kB p65 (OZYME, 9246S), and Actin (OZYME, 4967).

## Statistical Analysis

All quantitative data are presented as mean ± SEM from at least three independent experiments. Statistical significance was assessed using unpaired two-tailed Student's t-tests with unequal variance, unless otherwise specified. GraphPad Prism 7 (GraphPad Software) was used for statistical analysis, and p-values < 0.05 were considered statistically significant.

# Supplementary Information

## Supplementary Note 1. Description of the computational model

Following previous modeling studies of $Ca^{2+}$ dynamics (Voorsluijs et al., 2019; Ornelas-Guevara et al. 2023), we implement a fully stochastic model of intracellular $Ca^{2+}$ dynamics using the Gillespie algorithm. The model captures $IP_3$-induced $Ca^{2+}$ release from $IP_3R$ clusters, SERCA-mediated reuptake, ER $Ca^{2+}$ leak, and cytosolic $Ca^{2+}$ diffusion. The simulated HeLa cell is represented as a $10 \times 10$ $\mu m^2$ square, discretized into a $20 \times 20$ grid. Each compartment ($0.5 \times 0.5$ $\mu m^2$) corresponds to a cytosolic volume of $10^{-16}$ L.

Each $IP_3R$ cluster is represented as a single unit with four discrete states: Open (**O**), Closed (**C**), and two inhibited states ($\mathbf{i_1}$, $\mathbf{i_2}$). The transition from **C** to **O** depend on both [$Ca^{2+}$] and [$IP_3$], while the transition from **O** to **i1** depends on [$Ca^{2+}$], following the model described in Ornelas-Guevara et al.,

2023 (see Note1. Figure 1). Various spatial distributions of the $IP_3R$ clusters are investigated in Figure 5A to 5C, where the locations of the clusters are indicated by white boxes. SERCA activity and ER $Ca^{2+}$ leak are present in all compartments.

We use an extensivity parameter Ω to convert molecular counts to μM concentrations:

$$\Omega = N_A V_C \times 10^{-16} \mathrm{L}\mu\mathrm{mol}^{-1}$$

where $N_A$ is Avogadro's number and $V_C$ is the volume of each compartment.

The pseudocolor maps shown in Figure 5 display the maximum $\Delta[Ca^{2+}]/[Ca^{2+}]_b$ reached in each compartment during the simulation. These maps are intended to visualize the spatial distribution of the zones of $IP_3R$-mediated $Ca^{2+}$ release. The algorithm was implemented in MATLAB R2021b.

## Supplementary Note 2. Dependency of the effective $Ca^{2+}$ diffusion coefficient on $Ca^{2+}$ concentration

While in pure water the diffusion coefficient of $Ca^{2+}$ is very large (~500 $\mu m^2 s^{-1}$), in the cytoplasm it was reported to be in the range of 13-65 $\mu m^2 s^{-1}$, mainly due to interactions with $Ca^{2+}$ buffers (Allbritton et al., 1992). This value was determined experimentally by injecting large amounts of $^{45}Ca^{2+}$ at one end of a test tube filled with cytosolic extracts from *Xenopus* oocytes and measuring the spatial spread of radioactivity with time. Such measurements did not assess the dependency of the diffusion coefficient on the $Ca^{2+}$ concentration. A theoretical expression for the effective diffusion coefficient of $Ca^{2+}$ in the presence of buffers under the fast-buffering approximation was derived by Wagner and Keizer (1994). This expression was later shown by Smith et al. (1996) to be valid for a large range of buffering conditions. In this framework, the effective diffusion coefficient is given by

$$D_{eff} = \frac{D_C + \sum_{i=1}^{N} D_{B_i} \theta_i(c)}{1 + \sum_{i=1}^{N} \theta_i(c)}$$

with

$$\theta_i(c) = \frac{B_{T,i} K_{d,i}}{(K_{d,i} + c)^2}$$

Here, $D_C$ is the diffusion coefficient of free $Ca^{2+}$, $D_{Bi}$ is the diffusion coefficient of buffer species $i$, $B_{T,i}$ is the total concentration of buffer $i$, $K_{d,i}$ is its $Ca^{2+}$-binding affinity, and $c$ denotes the free $Ca^{2+}$ concentration. The dimensionless quantity $\theta_i(c)$ is the buffering capacity of species $i$.

It is worth mentioning that using the fast-buffer approximation is justified because the $Ca^{2+}$–buffer reaction takes place much faster than $Ca^{2+}$ diffuses over the relevant spatial scales. The characteristic reaction relaxation time can be estimated as $\tau_{relax} \approx 1/(k_{on} \cdot B_{tot} + k_{off})$, whereas the diffusion timescale over a distance L is $t_D \approx L^2/D_c$. For representative values ($k_{on}$ = 100 $\mu M^{-1} \cdot s^{-1}$, $B_{tot}$ = 15 μM, $K_d$ = 10 μM so $k_{off} = K_d \cdot k_{on}$ = 1000 $s^{-1}$), $\tau_{relax} \approx 1/(100\ \mu M^{-1} \cdot s^{-1} \cdot 15\ \mu M + 1000\ s^{-1}) \approx 4 \times 10^{-4}$ s. Over L = 5 μm, $t_D = 5^2/D_c$, which for $D_c$ = 220 $\mu m^2/s$ gives $t_D \approx 0.11$ s. Thus, $\tau_{relax}$ is ~300-fold shorter than $t_D$, so for practical purposes the fast-buffer approximation holds in this regime.

Immobile ($D_{Bii}$ = 0) or slowly diffusing buffers (small $D_{Bii}$) slow down the redistribution of $Ca^{2+}$ and therefore reduce the effective diffusion coefficient $D_{eff}$ in the $Ca^{2+}$ concentration ranges around and larger than their $K_d$. In contrast, fast buffers (large $D_{Bii}$) can transport $Ca^{2+}$ away from the source and effectively increase $Ca^{2+}$ mobility. When several buffers with different $K_{d,i}$, $B_{T,i}$, and $D_{Bi}$ coexist, their combined effect can make $D_{eff}(c)$ a non-monotonic function of $[Ca^{2+}]$, such that effective $Ca^{2+}$ diffusion coefficient can be larger or smaller than the diffusion coefficient estimated in the experiments of Allbritton et al. (1992).

To illustrate how this mechanism can generate concentration-dependent $Ca^{2+}$ mobility, we consider a simple but physiologically plausible mixture of three buffers with distinct properties chosen to be broadly consistent with well-known cytosolic $Ca^{2+}$-binding proteins (e.g., calbindin-D28k, calmodulin, and parvalbumin; Eisner et al., 2023).

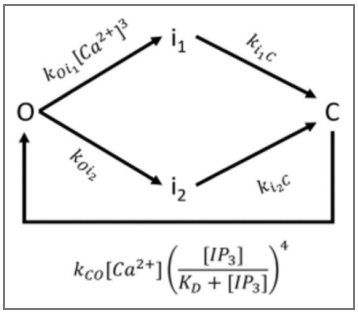


**Note 1. Figure 1. Model describing the dynamics of a cluster of $IP_3Rs$.**

From Ornelas-Guevara et al. (2023). $Ca^{2+}$ diffusion is modelled as a stochastic jump between adjacent compartments (Kraus et al., 1996). The propensity of a $Ca^{2+}$ ion to move depends on the deterministic diffusion coefficient (100 μm²/s) and concentration gradients, assuming isotropic and homogeneous diffusion. All reaction and diffusion events are simulated using the Gillespie algorithm. At each step, an event is selected probabilistically based on its propensity (See propensity functions in Note1. Table 1)

**Note 1. Table 1.** **Propensity functions and action of each process.**

$N_{ca,i}$ and $N_{ca,j}$ represent the number of ions in the current box (i) and in an adjacent box (j) selected randomly.

| Process | Propensity function | Action |
|---|---|---|
| 1. $Ca^{2+}$ diffusion | $4\frac{D_C}{\Delta x^2}N_{ca,i}$ | $N_{ca,i}-1$<br>$N_{ca,j}+1$ |
| 2. SERCA pumps | $\Omega\frac{v_p N_{ca,i}(N_{ca,i}-1)}{(K_p\Omega)^2+N_{ca,i}(N_{ca,i}-1)}$ | $N_{ca,i}-1$ |
| 3. Leak from the ER | $\Omega\frac{v_p[Ca^{2+}]_b^2}{{K_p}^2+[Ca^{2+}]_b^2}$ | $N_{ca,i}+1$ |
| 4. $C\rightarrow O$ | $k_{co}\frac{N_{ca,i}}{\Omega}\left(\frac{[IP_3]}{[IP_3]+K_D}\right)^4(N_{Vc}-N_{o,i}-N_{i1,i}-N_{i2,i})$ | $N_{o,i}=1$<br>$N_{c,i}=0$ |
| 5. $O\rightarrow i_1$ | $k_{oi1}N_{o,i}\frac{N_{ca,i}(N_{ca,i}-1)(N_{ca,i}-2)}{\Omega^3}$ | $N_{o,i}=0$<br>$N_{i1,i}=1$ |
| 6. $O\rightarrow i_2$ | $k_{oi1}N_{o,i}$ | $N_{o,i}=0$<br>$N_{i2,i}=1$ |
| 7. $i_1\rightarrow C$ | $k_{i1c}N_{i1,i}$ | $N_{i1,i}=0$<br>$N_{c,i}=1$ |
| 8. $i_2\rightarrow C$ | $k_{i2c}N_{i2,i}$ | $N_{i2,i}=0$<br>$N_{c,i}=1$ |
| 9. $Ca^{2+}$ release | $\Omega\Sigma\frac{N_{o,i}}{N_{Vc}}$ | $N_{ca,i}+1$ |

**Note 1. Table 2.** **Parameter values used for the simulations shown in Figure 5.**

| | | |
|---|---|---|
| $k_{co}$ | $12.5\ \mu M^{-1}s^{-1}$ | $C\rightarrow O$ |
| $k_{oi1}$ | $0.0125\ \mu M^{-3}s^{-1}$ | $O\rightarrow i_1$ |
| $k_{oi2}$ | $10\ s^{-1}$ | $O\rightarrow i_2$ |
| $k_{i1c}$ | $0.00125\ s^{-1}$ | $i_1\rightarrow C$ |
| $k_{i2c}$ | $0.5\ s^{-1}$ | $i_2\rightarrow C$ |
| $v_p$ | $0.225\ \mu M s^{-1}$ | Maximal rate of SERCA |
| $K_p$ | $0.1\ \mu M$ | SERCA binding constant |
| $K_D$ | $0.1\ \mu M$ | Affinity of $IP_3$Rs for $IP_3$ |
| $[Ca^{2+}]_b$ | $0.04\ \mu M$ | Basal cytosolic $[Ca^{2+}]$ |
| $D_C$ | $100\ \mu m^2 s^{-1}$ | $Ca^{2+}$ diffusion coefficient |
| $\Delta x$ | $0.5\mu m$ | Length of a compartment |
| $V_c$ | $10^{-16}\ L$ | Volume of a compartment |

· **Buffer 1**: immobile, low-affinity buffer

$$K_{d,1} = 10\mu M, \quad B_{T,1} = 15\mu M, \quad D_{B_1} = 0\mu m^2/s$$

· **Buffer 2**: mobile, moderate-affinity buffer

$$K_{d,2} = 10\mu M, \quad B_{T,2} = 85\mu M, \quad D_{B_2} = 15\mu m^2/s$$

· **Buffer 3**: mobile, high-affinity buffer

$$K_{d,3} = 0.1\mu M, \quad B_{T,3} = 15\mu M, \quad D_{B_3} = 120\mu m^2/s$$

These parameters are not meant to represent specific molecules, but to span a realistic range: an immobile buffer, a generic mobile $Ca^{2+}$ buffer (with a diffusion coefficient on the order of 10–20 μm$^2$/s), and a fast-diffusing $Ca^{2+}$ ligand (with a larger diffusion coefficient and lower concentration, conceptually similar to ADP). Many endogenous $Ca^{2+}$-binding species, including both proteins and small metabolites, fall within or between these regimes and, collectively, can act either as “sinks” that confine $Ca^{2+}$ or as “carriers” that help it spread.

Note 2. Figure 1 shows $D_{\text{eff}}(c)$ computed from the expressions given above for this buffer mixture. Because different buffers have different $K_d$ and $D_B$, the effective diffusion coefficient value varies with $c$ in a non-monotonic way: at some [$Ca^{2+}$] ranges, immobile or slow buffers dominate and reduce $Ca^{2+}$ mobility, whereas at other ranges the contribution of fast mobile carriers is more prominent and increases $D_{\text{eff}}$.

To connect this analysis with spatial [$Ca^{2+}$] profiles, we simulated $Ca^{2+}$ release from a point source in a two-dimensional reaction–diffusion system, including explicit $Ca^{2+}$–buffer binding (i.e. not using the equation to calculate $D_{\text{eff}}$ directly, but the underlying reaction–diffusion equations including $Ca^{2+}$-buffers binding and unbinding with the same parameters as in Note2. Fig. 1A). We considered two cases: a small-amplitude $Ca^{2+}$ release (Note2. Fig. 1B), and a large-amplitude $Ca^{2+}$ release (Note2. Fig. 1C), both with identical buffer parameters and diffusion coefficients. Note 2. Figures 2B and 2C show the resulting [$Ca^{2+}$] profiles 10 ms after release.

This example illustrates that, in the presence of multiple buffers with different kinetics and mobilities, low-amplitude $Ca^{2+}$ elevations can spread further than high-amplitude $Ca^{2+}$ signals. The reason is that low [$Ca^{2+}$] transients are handled mainly by fast, mobile buffers, whereas higher [$Ca^{2+}$] transients increasingly engage slowly diffusing buffers, which then dominate and reduce $Ca^{2+}$ mobility, confining the signal.

Importantly, this is not a universal statement about all possible buffer mixtures, but a specific example showing how realistic combinations of mobile and immobile buffers can produce a situation in which lower-amplitude $Ca^{2+}$ signals have a larger spatial extent than higher-amplitude $Ca^{2+}$ signals.

## Supplementary Note 3. Global $Ca^{2+}$ responses in the $IP_3R$ cluster model at higher stimulation and stronger $Ca^{2+}$ buffering

In the stochastic cluster model used in Fig. 5, $IP_3R$ clusters are represented at discrete spatial sites. Each cluster senses the local $Ca^{2+}$ concentration and its stochastic gating depends on this local [$Ca^{2+}$] and on [$IP_3$]. Buffers are not included explicitly. Instead, $Ca^{2+}$ diffusion in the cytosol is described by $D_{\text{eff}}$, which accounts for the combined action of endogenous $Ca^{2+}$-binding species.

In the regime relevant for CCRICs, we use $D_{\text{eff}}$ = 100 μm$^2$/s and a sub-threshold [$IP_3$] = 0.07 μM, below the level that produces global $Ca^{2+}$ responses in the model. With these values the model reproduces key properties of CCRICs: fast kinetics, small amplitude, and large spatial extent.

To simulate the behaviour of the model at higher IP3 stimulation levels, above-threshold $IP_3$ concentration, we increased [$IP_3$] to 0.1 μM (kept constant in time and space) and used a smaller effective diffusion coefficient, $D_{\text{eff}}$ = 40 μm$^2$/s expected for the stronger buffering and lower $Ca^{2+}$ mobility with higher-amplitude $Ca^{2+}$ signals (Note 2. Fig. 1).

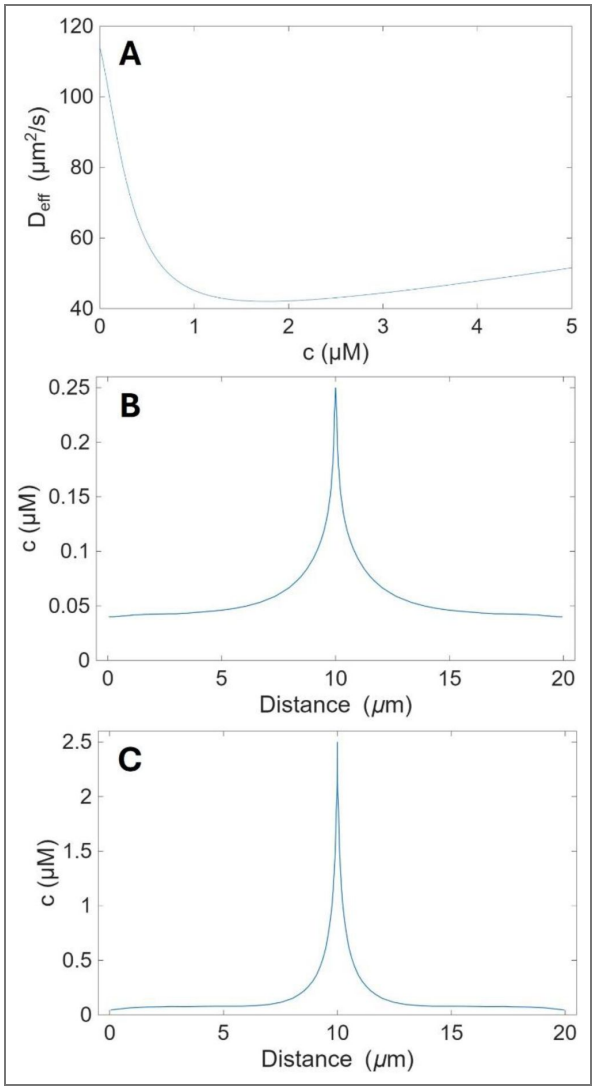


**Note 2. Figure 1.**

**A**, Effective diffusion coefficient of $Ca^{2+}$ ($D_{eff}$) as a function of free cytosolic [$Ca^{2+}$] (c) for a mixture of three buffers. Buffer 1 is immobile and low-affinity ($K_d$ = 10 μM, total concentration 15 μM, diffusion coefficient 0 μm²/s). Buffer 2 is mobile and has moderate affinity ($K_d$ = 10 μM, total concentration 85 μM, diffusion coefficient 15 μm²/s). Buffer 3 is highly mobile and has a high affinity ($K_d$ = 0.1 μM, total concentration 15 μM, diffusion coefficient 120 μm²/s). **B, C**, Spatial profiles of free [$Ca^{2+}$] 10 ms after a constant point-source release in the centre of a 10 × 10 μm² domain representing a cell, obtained from a two-dimensional reaction–diffusion simulation with explicit $Ca^{2+}$–buffer binding using the same buffer parameters as in (A). Only $Ca^{2+}$ release and binding to buffers were included in the simulation. The rate of $Ca^{2+}$ release is 10 times larger in C than in B. [$Ca^{2+}$] peaks at 0.25 μM (**B**) and 2.5 μM (**C**).

Under these conditions, the same cluster model generates a global $Ca^{2+}$ response with larger amplitude and longer duration, rather than a loss of activity due to excessive inhibition of the clusters (Figure S3A). Thus, within a single modelling framework, low $[IP_3]$ and $D_{eff}$ = 100 μm$^2$/s give rise to CCRIC-like responses, whereas higher $[IP_3]$ and a more strongly buffered regime ($D_{eff}$ = 40 μm$^2$/s) produce robust global $Ca^{2+}$ signals, comparable to global responses observed experimentally (Note 3. Fig. 1).

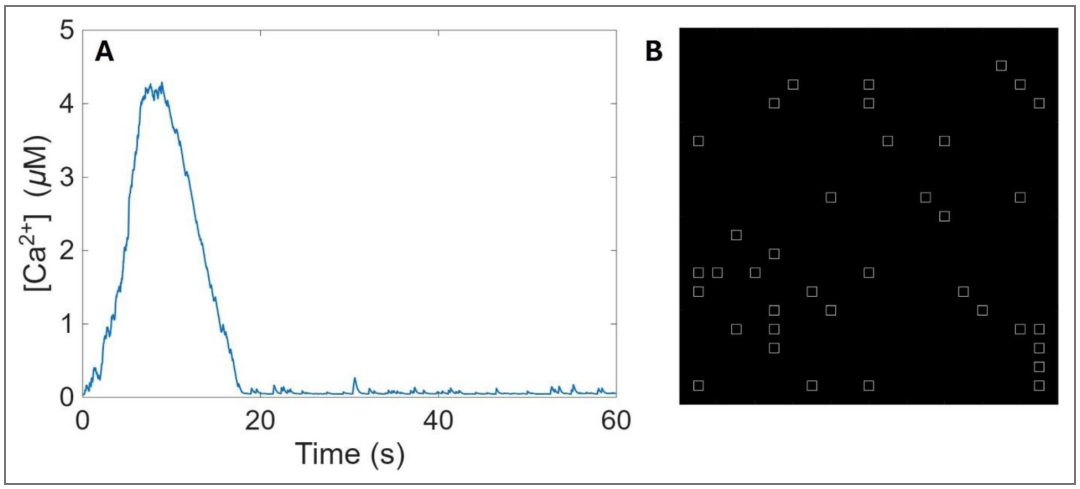


**Note 3. Fig. 1. Global $Ca^{2+}$ response at higher $[IP_3]$. A**, Time course of the averaged cytosolic $[Ca^{2+}]$ obtained from the stochastic $IP_3R$ cluster model for a uniform $[IP_3]$ = 0.1 μM and an effective diffusion coefficient $D_{eff}$ = 40 μm$^2$/s. All other parameters are identical to those used in the simulations shown in Fig. 5. Under these conditions, as opposed to CCRICs, the model produces a "classical" global $Ca^{2+}$ response with larger amplitude and long duration. **B**, 2D cell geometry (10 × 10 μm²) used in the simulations. Squares indicate the random positions of $IP_3R$ clusters.

# Supplementary figures

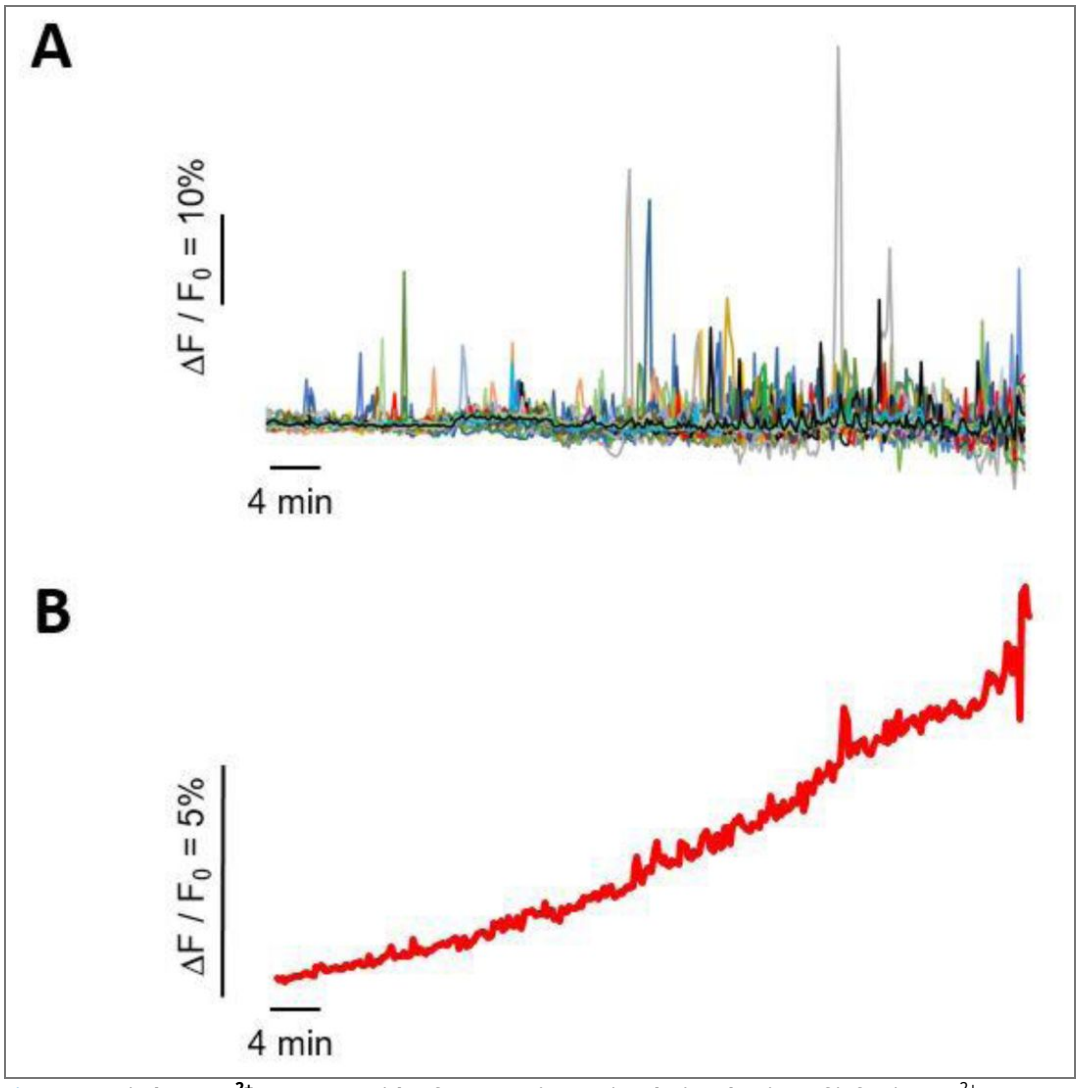


**Fig. S1. EPEC induces $Ca^{2+}$ responses with a frequency increasing during the time of infection.** $Ca^{2+}$ imaging was performed on HeLa cells loaded with the $Ca^{2+}$ fluorescent indicator Cal-520 and challenged with EPEC at a MOI of 100. A, Traces of $Ca^{2+}$ variations in single cells. B, Trace corresponding to the average of traces shown in B (N = 2, cells = 43). Note that cells do not show an increase in basal $Ca^{2+}$ levels that could be mistakenly interpreted from the averaging of $Ca^{2+}$ responses over the cell population.

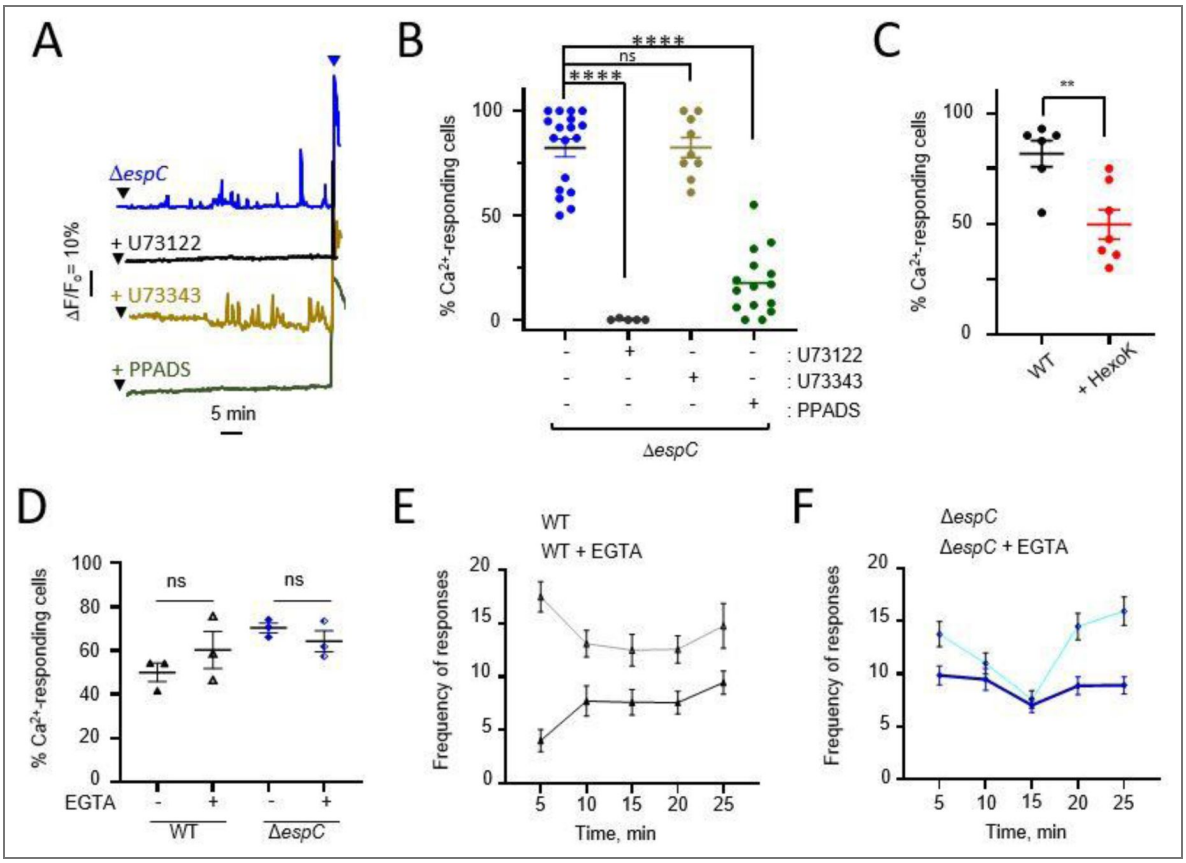


**Fig. S2. EPEC-induced $Ca^{2+}$ responses does not depend on $Ca^{2+}$ influx but on $Ca^{2+}$ release.**

HeLa cells were loaded with the fluorescent indicator Cal-520, challenged with a high MOI of EPEC wild-type (WT) or a low MOI of the *ΔespC* mutant and subjected to live-cell $Ca^{2+}$ imaging at a frequency of one acquisition every 10 seconds (**A-C**). **A**, Representative traces of $Ca^{2+}$ variations in single cells. The black arrowheads indicate the time of bacterial challenge. The blue arrowheads indicate stimulation with 3 µM histamine. **B**, Percent of cells exhibiting $Ca^{2+}$ responses. Cells challenged with: *ΔespC* (N = 4, cells > 400); + U73122: *ΔespC* in the presence of 10 µM U73122 (N = 4, cells > 160); + U73343: *ΔespC* in the presence of 10 µM U73343 (N = 2, cells = 230); + PPADS: *ΔespC* in the presence of 20 µM PPADS (N = 4, cells > 400). **C**, cells challenged with wild-type EPEC in the absence or presence of + hexokinase (200 units/ml) and 5 mM glucose (+ HexoK, N = 3, cells > 120). **D-F**, + EGTA: cells treated with 4 mM EGTA. (N = 3, cells > 30). **D**, Percent of cells showing $Ca^{2+}$ responses. **E**, **F**, Frequency of $Ca^{2+}$ responses per cell. Mann-Whitney test. ns: not significant. **: $p < 0.01$; ****: $p < 0.0001$.

**Figure S3. Suramin does not affect EPEC-Induced actin pedestals**

HeLa cells were challenged with the indicated RFP-expressing bacterial strains in the presence or absence of 100 µM suramin. Samples were fixed and processed for fluorescence staining. **A**, Representative micrographs. Blue: DAPI; green: Phalloidin-Alexa488; red: bacteria. Scale bar = 10 µm. **B**, Percent of cells exhibiting actin-rich pedestals. High MOI: 50 bacteria / cell. Low MOI *ΔespC*: 10 bacteria / cell. (N=3, n > 150). Mann Whitney test. ns: not significant.

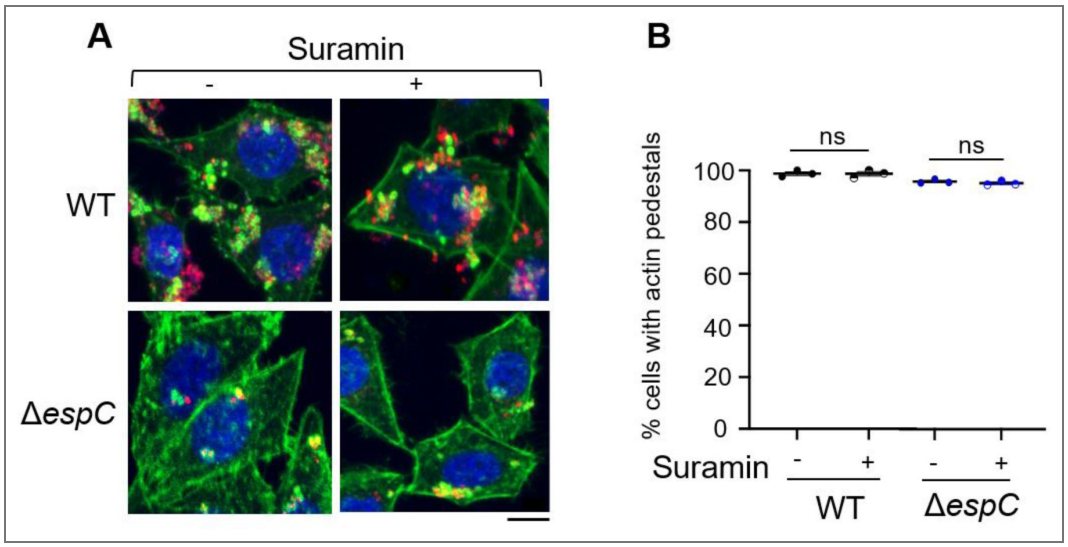


**Fig. S4. Low concentrations of histamine also induce small and fast coordinated $Ca^{2+}$ responses.**

HeLa cells were loaded with the fluorescent indicator Cal-520, challenged with 100 nM histamine and subjected to $Ca^{2+}$ imaging, with image acquisition performed every 57 ms. Left: fluorescence micrograph of the single cell with black and red ROIs corresponding to the traces of $Ca^{2+}$ variations in matching color. The box corresponds to a higher magnification of the inset in traces shown at the bottom. Arrowhead: challenge with 10 µM histamine. Traces are representative of 340 cells analyzed from 2 independent experiments, with a frequency of 4.5 ± 0.4 peaks·min$^{-1}$ (mean ± SEM) and peak duration of 4.45 ± 0.19 s (mean ± SEM).

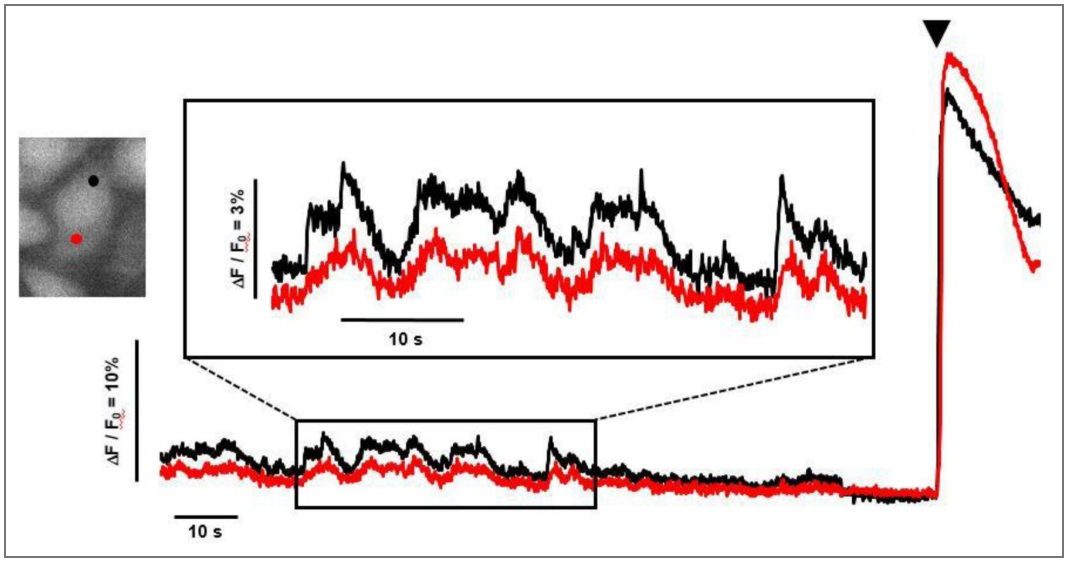

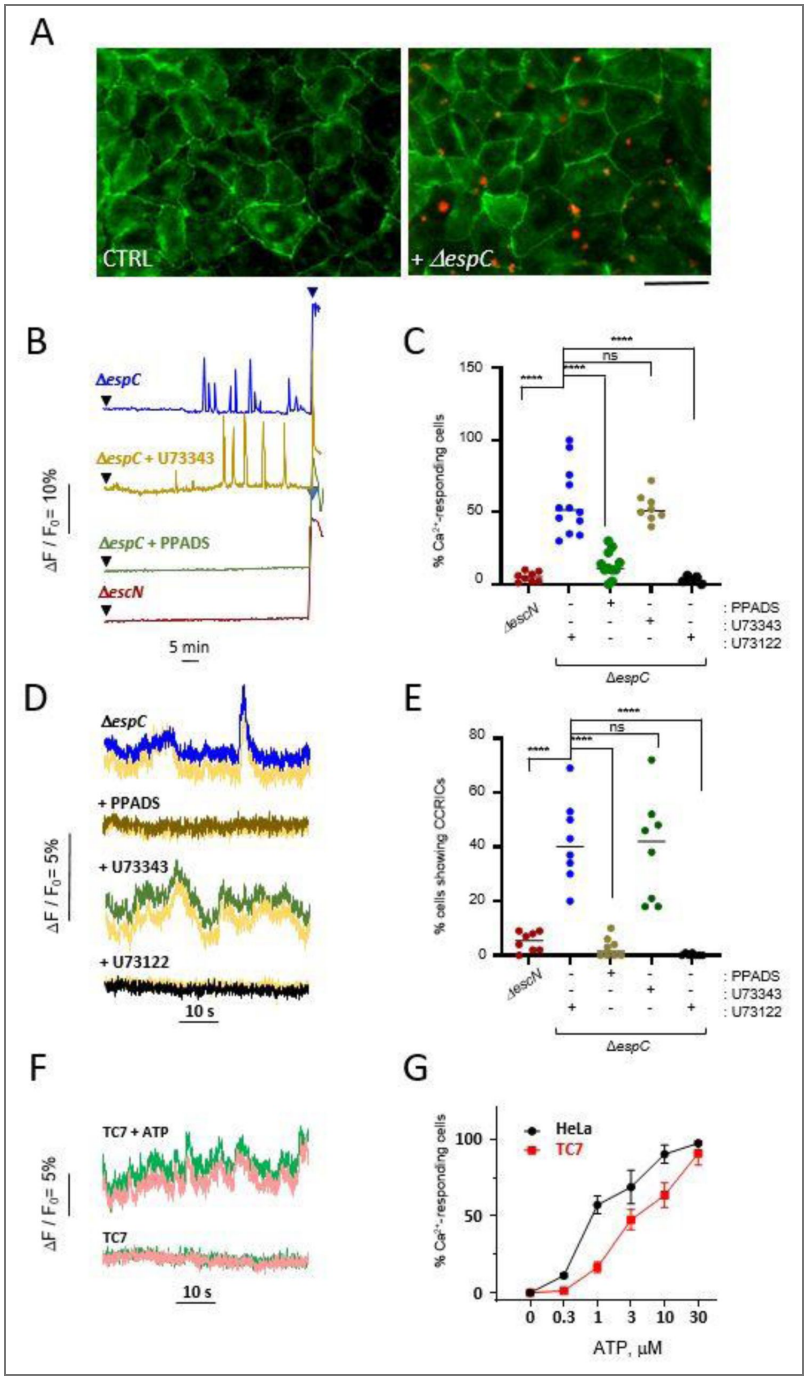


**Fig. S5. EPEC induces CRICCs in polarized intestinal cells via eATP release**

Polarized TC7 cells were loaded with the fluorescent indicator Cal-520 were challenged with the EPEC *ΔespC* strain expressing the Red Fluorescent Protein (RFP) (**A**-**E**) or with ATP (**F**, **G**). **A**, Representative confocal micrographs. Samples were, fixed and processed for fluorescence microscopy analysis. Green: ZO-1 staining. Red: RFP fluorescence. Scale bar = 10 µm. **B-G**, Samples were subjected to live-cell $Ca^{2+}$ imaging at a frequency of one acquisition every 5 seconds. **B**, **D**, Representative traces of $Ca^{2+}$ variations in single cells challenged with the indicated strain and inhibitor. The black arrowheads indicate the time of bacterial challenge. The blue arrowhead indicates stimulation with 3 µM histamine. **C**, **E**, Percent of cells exhibiting $Ca^{2+}$responses (**C**) (N = 4, cells > 241) or CCRICs (**E**) (N =3, cells > 66) following challenge with the indicated bacterial strain and inhibitor. Each value corresponds to a replicate. Mann-Whitney test. ****: $p < 0.0001$. **F**, Representative traces of $Ca^{2+}$ variations following challenge with 150 nM ATP (TC7 + ATP) or in buffer alone (TC7). The pink and green traces correspond to $Ca^{2+}$ variations in ROIs within the same cell. **G**, Percent of cells exhibiting $Ca^{2+}$responses following challenge with the indicated ATP concentration. Each value represents the mean ± SEM of at least 140 cells in 3 independent experiments.

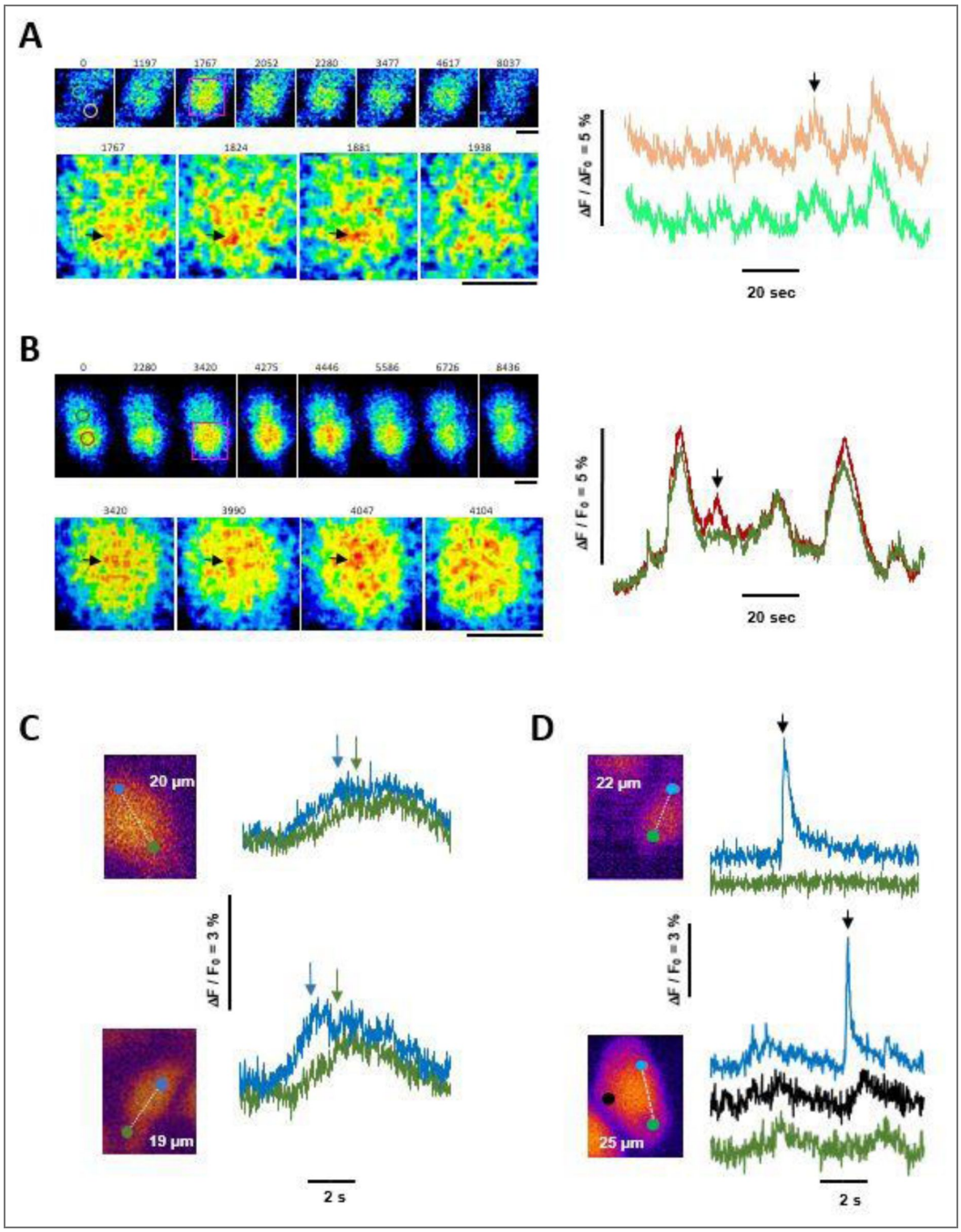


**Fig. S6. CCRICs induced by EPEC result from $Ca^{2+}$ released by highly transient or mobile $IP_3R$ clusters.**

HeLa cells were loaded with Cal-520 and challenged with wild type EPEC at a MOI of 50 bacteria / cell. **A**, **B**, Globally Coordinated responses associated with small and highly mobile clusters. **Time series micrographs**, Cal-520 intensity depicted in pseudocolor. Numbers: time in ms. Lower Panels are magnification of the purple box in the upper panel, with a time interval of 57 ms. Scale bar = 5 µm. Note the high mobility of small clusters / channels. The black arrows point at larger and less mobile clusters. **Traces**, variations of $Ca^{2+}$ in ROI depicted at T = 0 in the micrographs in the corresponding color. The black arrow points at the response peak illustrated by the time series. **C**, **D**, micrographs, Cal-520 fluorescence depicted in the Fiji red lute. Images were taken every 22 ms. Solid circles: ROIs where the variations of $Ca^{2+}$ are shown in traces in the corresponding on the right. The blue ROI correspond to the $Ca^{2+}$ release source based on the higher response amplitude, and the green ROI to a distal region. The number indicates the distance between the ROIs shown by the dashed line. **C**, Arrows point at the peak of the response in the ROI with the corresponding color. Note the delay in response elicitation between the source- (blue) and distal (green) ROI. **D**, Puff-like responses (black arrowhead). Note the absence of $Ca^{2+}$ variations in the distal region (Top), and the simultaneous elicitation of a puff and CCRICs in different ROIs (Bottom).

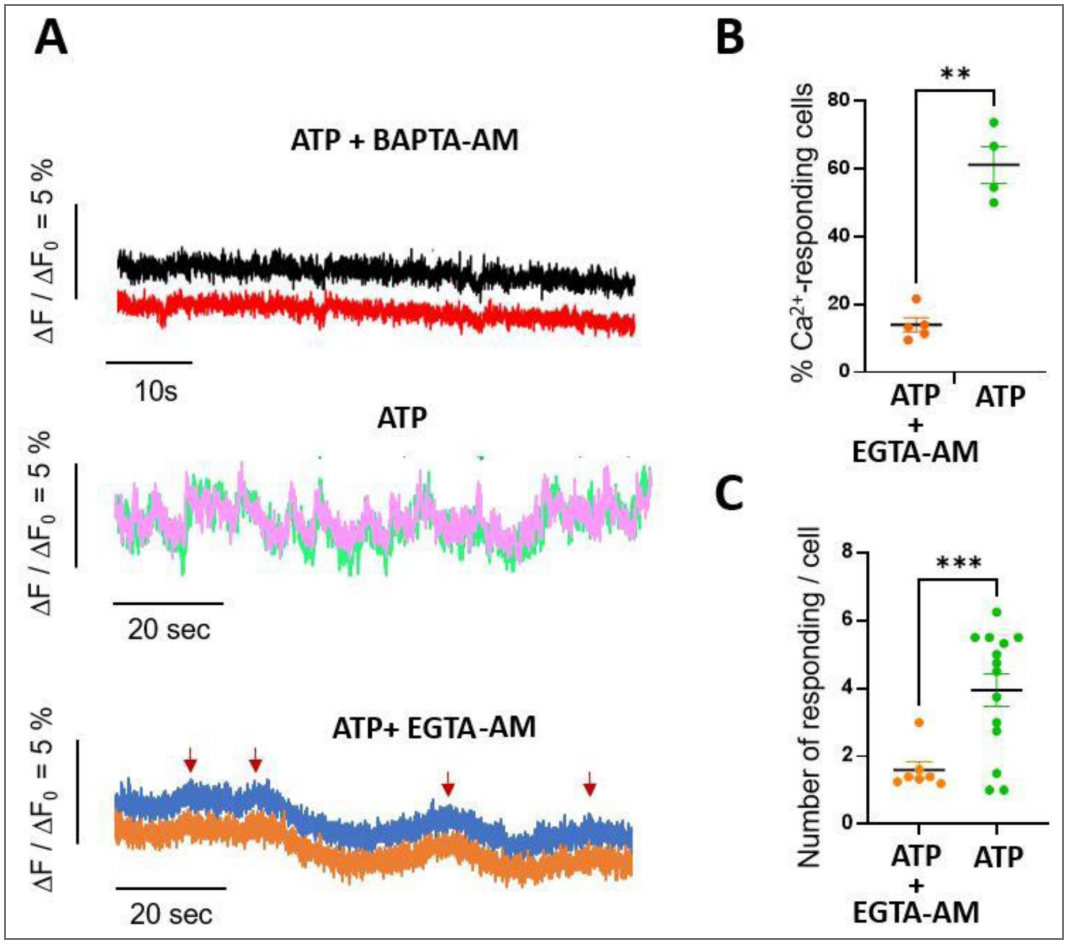


**Fig. S7. Intracellular $Ca^{2+}$ chelation inhibits CCRICs.**

HeLa cells were loaded with the fluorescent indicator Cal-520 in the presence or absence of 20 μM EGTA-AM or BAPTA-AM. Samples were stimulated with 150 nM ATP and subjected to high speed $Ca^{2+}$ imaging at a frequency of one acquisition every 22 ms. **A**, Representative traces of $Ca^{2+}$ variations in 2 subcellular regions of the same cell in samples treated in the presence or absence of the indicated inhibitor. No $Ca^{2+}$ responses were observed for cells treated with BAPTA-AM (N = 3, > 65 cells). EGTA-AM treatment led to an inhibition of $Ca^{2+}$ responses, associated with small variations in the $Ca^{2+}$ baseline that were arbitrarily scored as flattened $Ca^{2+}$ pseudo-responses (ATP+EGTA-AM, red arrows). **B**, Percent of cells exhibiting $Ca^{2+}$ responses (N > 3, cells > 62). **C**, average number of responses per cell. (N > 3, n > 62). Mann-Whitney test. **: $p < 0.01$; ***: $p < 0.001$.

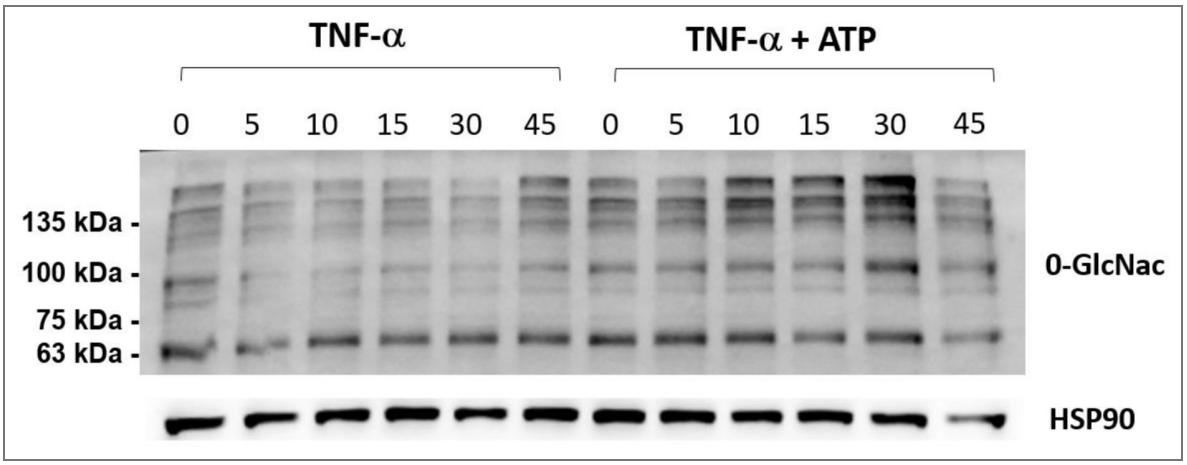


**Fig. S8. Effects of ATP on TNF-α-induced profiles of O-GlcNacylation in HeLa cells.**

HeLa cells were stimulated with 10 ng/ml TNF-α alone or co-stimulated with 10 ng/ml TNF-α and 150 nM ATP. Representative blots of cell lysates analyzed by Western blot at the time points indicated in minutes using the indicated antibodies.

## Data availability

Data associated with this article are available upon request.

## Acknowledgements

This work was funded by the Inserm, CNRS and ANR grants CalplyCx (ANR-20-CE15-0001), Vital (ANR-24-CE11-3941) to GTVN. FG was funded by a Chinese Science Council PhD fellowship. ROG was supported by Wallonie-Bruxelles International (Excellence Grant 2025). This work was supported by a PDR FRS-FNRS project (T.0073.21). GD is Research Director at the Belgian "Fonds National pour la Recherche Scientifique" (FRS-FNRS).

## Additional information

### Author contribution

FR, LC and GTVN designed, performed experiments and wrote the manuscript. LO performed experiments. ROG and GD performed the mathematical modeling.

### Funding


| Funder | Grant reference number | Author |
|---|---|---|
| Agence Nationale de la Recherche (ANR) | ANR-20-CE15-0001 | Guy Tran Van Nhieu |
| Agence Nationale de la Recherche (ANR) | ANR-24-CE11-3941 | Guy Tran Van Nhieu |
| Wallonie-Bruxelles International (WBI) | Excellence Grant 2025 | Geneviève Dupont |
| Fonds De La Recherche Scientifique - FNRS (FNRS) | PDR T.0073.21 | Geneviève Dupont |
| China Scholarship Council (CSC) | PhD fellowship | Fangrui GUO |


### Author ORCID iDs

**Guy Tran Van Nhieu**: https://orcid.org/0000-0002-3901-2186

## References

1. **Abul-Milh M.,** Wu Y., Lau B., Lingwood C. A., Foster D. B (2001) Induction of Epithelial Cell Death Including Apoptosis by Enteropathogenic Escherichia coli Expressing Bundle-Forming Pili. *Infection and Immunity* **69**:7356-7364 https://doi.org/10.1128/IAI.69.12.7356-7364.2001 | PubMed
2. **Bain C,** Keller R, Collington GK, Trabulsi LR, Knutton S (1998) Increased levels of intracellular calcium are not required for the formation of attaching and effacing lesions by enteropathogenic and enterohemorrhagic Escherichia coli. *Infect Immun* **66**:3900-8 https://doi.org/10.1128/IAI.66.8.3900-3908.1998 | PubMed | PubMed Central
3. **Baldwin T. J.,** Ward W., Aitken A., Knutton S., Williams P. H (1991) Elevation of intracellular free calcium levels in HEp-2 cells infected with enteropathogenic Escherichia coli. *Infection and Immunity* **59**:1599-1604 https://doi.org/10.1128/iai.59.5.1599-1604.1991 | PubMed
4. **Baldwin TJ,** Lee-Delaunay MB, Knutton S, Williams PH (1993) Calcium-calmodulin dependence of actin accretion and lethality in cultured HEp-2 cells infected with enteropathogenic Escherichia coli. *Infect Immun* **61**:760-3 https://doi.org/10.1128/iai.61.2.760-763.1993 | PubMed | PubMed Central
5. **Brown MD,** Bry L, Li Z, Sacks DB (2008) Actin pedestal formation by enteropathogenic Escherichia coli is regulated by IQGAP1, calcium, and calmodulin. *J Biol Chem* **283**:35212-22 https://doi.org/10.1074/jbc.M803477200 | PubMed | PubMed Central

6. **Baruch K.,** Gur-Arie L., Nadler C., Koby S., Yerushalmi G., Ben-Neriah Y., Yogev O., Shaulian E., Guttman C., Zarivach R., *et al.* (2011) Metalloprotease type III effectors that specifically cleave JNK and NF-κB. *The EMBO Journal* **30**:221-231 https://doi.org/10.1038/emboj.2010.297 | PubMed
7. **Chatterjee A.,** Caballero-Franco C., Bakker D., Totten S., Jardim A (2015) Pore-forming Activity of the Escherichia coli Type III Secretion System Protein EspD. *The Journal of Biological Chemistry* **290**:25579-25594 https://doi.org/10.1074/jbc.M115.648204 | PubMed
8. **Chen H. D.,** Frankel G (2005) Enteropathogenic Escherichia coli: Unravelling pathogenesis. *FEMS Microbiology Reviews* **29**:83-98 https://doi.org/10.1016/j.femsre.2004.07.002 | PubMed
9. **Clapham D. E** (2007) Calcium Signaling. *Cell* **131**:1047-1058 https://doi.org/10.1016/j.cell.2007.11.028 | PubMed
10. **Crane J. K.,** Olson R. A., Jones H. M., Duffey M. E (2002) Release of ATP during host cell killing by enteropathogenicE. coli and its role as a secretory mediator. *American Journal of Physiology-Gastrointestinal and Liver Physiology* **283**:G74-G86 https://doi.org/10.1152/ajpgi.00484.2001 | PubMed
11. **Creasey E. A.,** Delahay R. M., Daniell S. J., Frankel G (2003) Yeast two-hybrid system survey of interactions between LEE-encoded proteins of enteropathogenic Escherichia coli. *Microbiology* **149**:2093-2106 https://doi.org/10.1099/mic.0.26355-0 | PubMed
12. **Croxen M. A.,** Law R. J., Scholz R., Keeney K. M., Wlodarska M., Finlay B. B (2013) Recent advances in understanding enteric pathogenic Escherichia coli. *Clinical Microbiology Reviews* **26**:822-880 https://doi.org/10.1128/CMR.00022-13 | PubMed
13. **Dong X.,** Shu L., Zhang J., Yang X., Cheng X., Zhao X., Qu W., Zhu Q., Shou Y., Peng G., *et al.* (2023) Ogt-mediated O-GlcNAcylation inhibits astrocytes activation through modulating NF-κB signaling pathway. *Journal of Neuroinflammation* **20**:146 https://doi.org/10.1186/s12974-023-02824-8 | PubMed
14. **Dupont G.,** Combettes L., Bird G. S., Putney J. W (2011) Calcium oscillations. *Cold Spring Harbor Perspectives in Biology* **3**:a004226 https://doi.org/10.1101/cshperspect.a004226 | PubMed
15. **Edwards L. A.,** Bajaj-Elliott M., Klein N. J., Murch S. H., Phillips A. D (2011) Bacterial-Epithelial Contact Is a Key Determinant of Host Innate Immune Responses to Enteropathogenic and Enteroaggregative Escherichia coli. *PLOS One* **6**:e27030 https://doi.org/10.1371/journal.pone.0027030 | PubMed
16. **Falcke M** (2003) Deterministic and stochastic models of intracellular $Ca^{2+}$ waves. *New J Phys* **5**:96 https://doi.org/10.1088/1367-2630/5/1/396
17. **Foskett J. K.,** White C., Cheung K.-H., Mak D.-O. D (2007) Inositol Trisphosphate Receptor Ca2+ Release Channels. *Physiological Reviews* **87**:593-658 https://doi.org/10.1152/physrev.00035.2006 | PubMed
18. **Foubister V,** Rosenshine I, Finlay BB (1994) A diarrheal pathogen, enteropathogenic Escherichia coli (EPEC), triggers a flux of inositol phosphates in infected epithelial cells. *J Exp Med* **179**:993-8 https://doi.org/10.1084/jem.179.3.993 | PubMed | PubMed Central
19. **Gao X.,** Wan F., Mateo K., Callegari E., Wang D., Deng W., Puente J., Li F., Chaussee M. S., Finlay B. B., *et al.* (2009) Bacterial Effector Binding to Ribosomal Protein S3 Subverts NF-κB Function. *PLoS Pathogens* **5**:e1000708 https://doi.org/10.1371/journal.ppat.1000708 | PubMed
20. **Giogha C.,** Lung T. W. F., Mühlen S., Pearson J. S., Hartland E. L (2015) Substrate recognition by the zinc metalloprotease effector NleC from enteropathogenic Escherichia coli. *Cellular Microbiology* **17**:1766-1778 https://doi.org/10.1111/cmi.12469 | PubMed
21. **Gomes T. A. T.,** Elias W. P., Scaletsky I. C. A., Guth B. E. C., Rodrigues J. F., Piazza R. M. F., Ferreira L. C. S., Martinez M. B (2016) Diarrheagenic Escherichia coli. *Brazilian Journal of Microbiology: [Publication of the Brazilian Society for Microbiology]* **47**:3-30 https://doi.org/10.1016/j.bjm.2016.10.015 | PubMed
22. **Guignot J.,** Segura A., Tran Van Nhieu G. (2015) The Serine Protease EspC from Enteropathogenic Escherichia coli Regulates Pore Formation and Cytotoxicity Mediated by the Type III Secretion System. *PLoS Pathogens* **11**:e1005013 https://doi.org/10.1371/journal.ppat.1005013 | PubMed

23. **Guignot J.,** Tran Van Nhieu G. (2016) Bacterial Control of Pores Induced by the Type III Secretion System: Mind the Gap. *Frontiers in Immunology* **7**:84 https://doi.org/10.3389/fimmu.2016.00084 | PubMed

24. **Hazen T. H.,** Donnenberg M. S., Panchalingam S., Antonio M., Hossain A., Mandomando I., Ochieng J. B., Ramamurthy T., Tamboura B., Qureshi S., *et al.* (2016) Genomic diversity of EPEC associated with clinical presentations of differing severity. *Nature Microbiology* **1**:15014 https://doi.org/10.1038/nmicrobiol.2015.14 | PubMed

25. **Jaiswal J. K.,** Andrews N. W., Simon S. M (2002) Membrane proximal lysosomes are the major vesicles responsible for calcium-dependent exocytosis in nonsecretory cells. *The Journal of Cell Biology* **159**:625-635 https://doi.org/10.1083/jcb.200208154 | PubMed

26. **Li S.,** Zhang L., Yao Q., Li L., Dong N., Rong J., Gao W., Ding X., Sun L., Chen X., *et al.* (2013) Pathogen blocks host death receptor signalling by arginine GlcNAcylation of death domains. *Nature* **501**:242-246 https://doi.org/10.1038/nature12436 | PubMed

27. **Liu A. R.,** Ramakrishnan P (2021) Regulation of Nuclear Factor-kappaB Function by O-GlcNAcylation in Inflammation and Cancer. *Frontiers in Cell and Developmental Biology* **9**:751761 https://doi.org/10.3389/fcell.2021.751761 | PubMed

28. **Lozer D. M.,** Souza T. B., Monfardini M. V., Vicentini F., Kitagawa S. S., Scaletsky I. C. A., Spano L. C (2013) Genotypic and phenotypic analysis of diarrheagenic Escherichia coli strains isolated from Brazilian children living in low socioeconomic level communities. *BMC Infectious Diseases* **13**:418 https://doi.org/10.1186/1471-2334-13-418 | PubMed

29. **Mills E.,** Baruch K., Charpentier X., Kobi S., Rosenshine I (2008) Real-time analysis of effector translocation by the type III secretion system of enteropathogenic Escherichia coli. *Cell Host & Microbe* **3**:104-113 https://doi.org/10.1016/j.chom.2007.11.007 | PubMed

30. **Monjarás Feria J.,** García-Gómez E., Espinosa N., Minamino T., Namba K., González-Pedrajo B (2012) Role of EscP (Orf16) in injectisome biogenesis and regulation of type III protein secretion in enteropathogenic Escherichia coli. *Journal of Bacteriology* **194**:6029-6045 https://doi.org/10.1128/JB.01215-12 | PubMed

31. **Motolani A.,** Martin M., Wang B., Jiang G., Alipourgivi F., Huang X., Safa A., Liu Y., Lu T (2023) Critical Role of Novel O-GlcNAcylation of S550 and S551 on the p65 Subunit of NF-κB in Pancreatic Cancer. *Cancers* **15**:4742 https://doi.org/10.3390/cancers15194742 | PubMed

32. **Ornelas-Guevara R,** Gil D, Voorsluijs V, Dupont G (2023) Computational investigation of $IP_3$ diffusion. *Sci Rep* **13**:2922 https://doi.org/10.1038/s41598-023-29876-3 | PubMed | PubMed Central

33. **Özcan S.,** Andrali S. S., Cantrell J. E. L (2010) Modulation of transcription factor function by O-GlcNAc modification. *Biochimica et Biophysica Acta* **1799**:353-364 https://doi.org/10.1016/j.bbagrm.2010.02.005 | PubMed

34. **Pallett M. A.,** Berger C. N., Pearson J. S., Hartland E. L., Frankel G (2014) The type III secretion effector NleF of enteropathogenic Escherichia coli activates NF-κB early during infection. *Infection and Immunity* **82**:4878-4888 https://doi.org/10.1128/IAI.02131-14 | PubMed

35. **Pearson J. S.,** Giogha C., Ong S. Y., Kennedy C. L., Kelly M., Robinson K. S., Lung T. W. F., Mansell A., Riedmaier P., Oates C. V. L., *et al.* (2013) A type III effector antagonizes death receptor signalling during bacterial gut infection. *Nature* **501**:247-251 https://doi.org/10.1038/nature12524 | PubMed

36. **Pearson J. S.,** Giogha C., Lung T. W. F., Hartland E. L (2016) The Genetics of Enteropathogenic Escherichia coli Virulence. *Annual Review of Genetics* **50** https://doi.org/10.1146/annurev-genet-120215-035138 | PubMed

37. **Ramachandran R. P.,** Spiegel C., Keren Y., Danieli T., Melamed-Book N., Pal R. R., Zlotkin-Rivkin E., Rosenshine I., Aroeti B (2020) Mitochondrial Targeting of the Enteropathogenic Escherichia coli Map Triggers Calcium Mobilization, ADAM10-MAP Kinase Signaling, and Host Cell Apoptosis. *mBio* e01397 https://doi.org/10.1128/mBio.01397-20 | PubMed

38. **Ruan H.-B.,** Ma Y., Torres S., Zhang B., Feriod C., Heck R. M., Qian K., Fu M., Li X., Nathanson M. H., *et al.* (2017) Calcium-dependent O-GlcNAc signaling drives liver autophagy in adaptation to starvation. *Genes & Development* **31**:1655-1665 https://doi.org/10.1101/gad.305441.117 | PubMed

39. **Ruchaud-Sparagano M.-H.,** Mühlen S., Dean P., Kenny B (2011) The enteropathogenic E. coli (EPEC) Tir effector inhibits NF-κB activity by targeting TNF-α receptor-associated factors. *PLoS Pathogens* **7**:e1002414 https://doi.org/10.1371/journal.ppat.1002414 | PubMed

40. **Sal-Man N.,** Deng W., Finlay B. B (2012) EscI: A crucial component of the type III secretion system forms the inner rod structure in enteropathogenic Escherichia coli. *The Biochemical Journal* **442**:119-125 https://doi.org/10.1042/BJ20111620 | PubMed

41. **Savio LEB,** de Andrade Mello P, da Silva CG, Coutinho-Silva R. (2018) The P2X7 Receptor in Inflammatory Diseases: Angel or Demon?. *Front Pharmacol* https://doi.org/10.3389/fphar.2018.00052 | PubMed | PubMed Central

42. **Serapio-Palacios A.,** Navarro-Garcia F (2016) EspC, an Autotransporter Protein Secreted by Enteropathogenic Escherichia coli, Causes Apoptosis and Necrosis through Caspase and Calpain Activation, Including Direct Procaspase-3 Cleavage. *mBio* **7**:e00479-16 https://doi.org/10.1128/mBio.00479-16 | PubMed

43. **Shtuhin-Rahav R.,** Olender A., Zlotkin-Rivkin E., Bouman E. A., Danieli T., Nir-Keren Y., Weiss A. M., Nandi I., Aroeti B (2023) Enteropathogenic E. coli infection co-elicits lysosomal exocytosis and lytic host cell death. *mBio* **14**:e01979-23 https://doi.org/10.1128/mbio.01979-23 | PubMed

44. **Smedler E,** Uhlén P (2014) Frequency decoding of calcium oscillations. *Biochim Biophys Acta* 964-9 https://doi.org/10.1016/j.bbagen.2013.11.015 | PubMed

45. **Swillens S,** Dupont G, Combettes L, Champeil P (1999) From calcium blips to calcium puffs: theoretical analysis of the requirements for interchannel communication. *Proc Natl Acad Sci U S A* **96**:13750-5 https://doi.org/10.1073/pnas.96.24.13750 | PubMed | PubMed Central

46. **Szabadkai G.,** Simoni A. M., Rizzuto R (2003) Mitochondrial Ca2+ uptake requires sustainedCa2+ release from the endoplasmic reticulum. *The Journal of Biological Chemistry* **278**:15153-15161 https://doi.org/10.1074/jbc.M300180200 | PubMed

47. **Tsunemi T.,** Perez-Rosello T., Ishiguro Y., Yoroisaka A., Jeon S., Hamada K., Rammonhan M., Wong Y. C., Xie Z., Akamatsu W., *et al.* (2019) Increased Lysosomal Exocytosis Induced by Lysosomal Ca2+ Channel Agonists Protects Human Dopaminergic Neurons from α-Synuclein Toxicity. *Journal of Neuroscience* **39**:5760-5772 https://doi.org/10.1523/JNEUROSCI.3085-18.2019 | PubMed

48. **Thomas D,** Lipp P, Tovey SC, Berridge MJ, Li W, Tsien RY, Bootman MD (2000) Microscopic properties of elementary Ca2+ release sites in non-excitable cells. *Curr Biol* **10**:8-15 https://doi.org/10.1016/s0960-9822(99)00258-4 | PubMed

49. **Vandeput F.,** Combettes L., Mills S. J., Backers K., Wohlkönig A., Parys J. B., De Smedt H., Missiaen L., Dupont G., Potter B. V. L., *et al.* (2007) Biphenyl 2,3',4,5',6-pentakisphosphate, a novel inositol polyphosphate surrogate, modulates Ca2+ responses in rat hepatocytes. *FASEB Journal: Official Publication of the Federation of American Societies for Experimental Biology* https://doi.org/10.1096/fj.06-7691com | PubMed

50. **Voorsluijs V,** Dawson SP, De Decker Y, Dupont G (2019) Deterministic Limit of Intracellular Calcium Spikes. *Phys Rev Lett* **122**:088101 https://doi.org/10.1103/PhysRevLett.122.088101 | PubMed

51. **Yan D.,** Quan H., Wang L., Liu F., Liu H., Chen J., Cao X., Ge B (2013) Enteropathogenic *Escherichia coli* Tir recruits cellular SHP-2 through ITIM motifs to suppress host immune response. *Cellular Signalling* **25**:1887-1894 https://doi.org/10.1016/j.cellsig.2013.05.020 | PubMed

52. **Yen H.,** Ooka T., Iguchi A., Hayashi T., Sugimoto N., Tobe T (2010) NleC, a Type III Secretion Protease, Compromises NF-κB Activation by Targeting p65/RelA. *PLOS Pathogens* **6**:e1001231 https://doi.org/10.1371/journal.ppat.1001231 | PubMed

53. **Zhang L.,** Ding X., Cui J., Xu H., Chen J., Gong Y.-N., Hu L., Zhou Y., Ge J., Lu Q., *et al.* (2011) Cysteine methylation disrupts ubiquitin-chain sensing in NF-κB activation. *Nature* **481**:204-208 https://doi.org/10.1038/nature10690 | PubMed

54. **Zhong Q.,** Roumeliotis T. I., Kozik Z., Cepeda-Molero M., Fernández L. Á., Shenoy A. R., Bakal C., Frankel G., Choudhary J. S (2020) Clustering of Tir during enteropathogenic E. coli infection triggers calcium influx–dependent pyroptosis in intestinal epithelial cells. *PLoS Biology* **18**:e3000986 https://doi.org/10.1371/journal.pbio.3000986 | PubMed

55. **Zhong Q.,** Chatterjee S., Choudhary J. S., Frankel G (2022) EPEC-induced activation of the Ca2+ transporter TRPV2 leads to pyroptotic cell death. *Molecular Microbiology* **117**:480-492 https://doi.org/10.1111/mmi.14863 | PubMed

56. **Allbritton N.,** Meyer T., Stryer L (1992) Range of messenger action of calcium ion and inositol 1,4,5-trisphosphate. *Science* https://doi.org/10.1126/science.1465619 | PubMed

57. **Eisner D.,** Neher E., Taschenberger H., Smith G (2023) Physiology of intracellular calcium buffering. *Physiological reviews* **103**:2767-2845 https://doi.org/10.1152/physrev.00042.2022 | PubMed

58. **Gillespie D** (1976) A general method for numerically simulating the stochastic time evolution of coupled chemical reactions. *Journal of Computational Physics* **22**:403-434 https://doi.org/10.1016/0021-9991(76)90041-3

59. **Kraus M.,** Wolf B., Wolf B (1996) Crosstalk between cellular morphology and calcium oscillation patterns. Insights from a stochastic computer model. *Cell Calcium* **19**:461-472 https://doi.org/10.1016/s0143-4160(96)90055-x | PubMed

60. **Ornelas-Guevara R.,** Gil D., Voorsluijs V., Dupont G (2023) Computational investigation of $IP_3$ diffusion. *Scientific Reports* **13**:2922 https://doi.org/10.1038/s41598-023-29876-3 | PubMed

61. **Smith G. D.,** Wagner J., Keizer J (1996) Validity of the rapid buffering approximation near a point source of calcium ions. *Biophysical journal* **70**:2527-2539 https://doi.org/10.1016/S0006-3495(96)79824-7 | PubMed

62. **Voorsluijs V.,** Ponce Dawson S., De Decker Y., Dupont G. (2019) Deterministic limit of intracellular calcium spikes. *Physics Review Letters* **122**:088101 https://doi.org/10.1103/physrevlett.122.088101 | PubMed

63. **Wagner J.,** Keizer J (1994) Effects of rapid buffers on $Ca^{2+}$ diffusion and $Ca^{2+}$ oscillations. *Biophysical journal* **67**:447-456 https://doi.org/10.1016/S0006-3495(94)80500-4 | PubMed

# Peer reviews

## Reviewer #1 (Public review):

Summary:

In their article, Guo and coworkers investigate the $Ca^{2+}$ signaling responses induced by Enteropathogenic Escherichia coli (EPEC) in epithelial cells and how these responses regulate NF-κB activation. The authors show that EPEC induces rapid, spatially coordinated $Ca^{2+}$ transients mediated by extracellular ATP released through the type III secretion system (T3SS). Using high-speed $Ca^{2+}$ imaging and stochastic modeling, they propose that low ATP levels trigger "Coordinated $Ca^{2+}$ Responses from $IP_3R$ Clusters" (CCRICs) via fast $Ca^{2+}$ diffusion and $Ca^{2+}$-induced $Ca^{2+}$ release. These responses may dampen TNF-α-induced NF-κB activation through $Ca^{2+}$-dependent modulation of O-GlcNAcylation of p65. The interdisciplinary work suggests a new perspective on calcium-mediated immune response by combining quantitative imaging, bacterial genetics, and computational modeling.

Strengths:

The study provides a new concept for host responses to bacterial infections and introduces the concept of Coordinated $Ca^{2+}$ Responses from $IP_3R$ Clusters (CCRICs) as synchronized, whole-cell-scale $Ca^{2+}$ transients with the fast kinetics typical of local events. This is elegantly done by an interdisciplinary approach using quantitative measurements and mechanistic modelling.

Comments on revised version.

The revised version of the manuscript has addressed all my raised points. I'd like to thank the authors for the work they have put into the revision to make this a very compelling publication.

https://doi.org/10.7554/eLife.108953.2.sa2

## Reviewer #2 (Public review):

Summary:

The authors of this study are trying to resolve how cellular infection by enteropathogenic E. coli (EPEC) subverts cellular signaling pathways to promote infection and dampen immune responses. Specifically, alteration in calcium dynamics has been evidenced in the prior literature as a potential initiator of these adaptions, and this study provides ideas and mechanistic detail as to how cellular calcium dynamics may be subverted by pathogens.

Strengths:

The clear strengths of this paper relate to the new ideas inherent in the proposed hypothesis and their support from the experimental approaches used. Overall, the proposed work provides new ideas in this area, which will benefit from further investigation. Certainly, this is an interesting and challenging paradigm to pick apart mechanistically, and is important for improving treatments from intestinal infections. The authors have provided additional data to clarify and expand on concerns raised during the original review, and these additions are helpful.

Comments on revised version.

Thorough response to original review. No further comments.

https://doi.org/10.7554/eLife.108953.2.sa1

## Author response:

The following is the authors' response to the original reviews.

> ***Public Reviews:***
>
> ***Reviewer #1 (Public review):***
>
> *Summary:*
>
> *In their article, Guo and coworkers investigate the $Ca^{2+}$ signaling responses induced by Enteropathogenic Escherichia coli (EPEC) in epithelial cells and how these responses regulate NF-κB activation. The authors show that EPEC induces rapid, spatially coordinated $Ca^{2+}$ transients mediated by extracellular ATP released through the type III secretion system (T3SS). Using high-speed $Ca^{2+}$ imaging and stochastic modeling, they propose that low ATP levels trigger "Coordinated $Ca^{2+}$ Responses from $IP_3R$ Clusters" (CCRICs) via fast $Ca^{2+}$ diffusion and $Ca^{2+}$-induced $Ca^{2+}$ release. These responses may dampen TNF-α-induced NF-κB activation through $Ca^{2+}$-dependent modulation of O-GlcNAcylation of p65. The interdisciplinary work suggests a new perspective on calcium-mediated immune response by combining quantitative imaging, bacterial genetics, and computational modeling.*
>
> *Strengths:*

> *The study provides a new concept for host responses to bacterial infections and introduces the concept of Coordinated $Ca^{2+}$ Responses from $IP_3R$ Clusters (CCRICs) as synchronized, whole-cell-scale $Ca^{2+}$ transients with the fast kinetics typical of local events. This is elegantly done by an interdisciplinary approach using quantitative measurements and mechanistic modelling.*
>
> *Weaknesses:*
>
> *(1) The effect of coordination by fast diffusion for small eATP concentrations is explained by the resulting low Ca2+ concentration that is not as strongly affected by calcium buffers compared to higher concentrations. While I agree with this statement on the relative level, CICR is based on the resulting absolute concentration at neighboring IP3Rs (to activate them). Thus, I do not fully agree with the explanation, or at least would expect to use the modelling approach to demonstrate this effect. Simulations for different activation and buffer concentrations could strengthen this point and exclude potential inhibition of channels at higher stimulation levels.*

We fully agree that CICR is determined by the local $Ca^{2+}$ concentration at each $IP_3R$ cluster, not by a global cytosolic average. In our stochastic model, $IP_3$ R clusters are represented as phenomenological entities at discrete spatial sites. Each cluster senses the local $Ca^{2+}$ concentration at its position, and its stochastic gating depends only on this local [$Ca^{2+}$] and on [IP3]. Buffers are not included explicitly. Instead, we use an effective Ca2+ diffusion coefficient Deff, which accounts for the effect of endogenous $Ca^{2+}$ buffers. To reproduce the coordinated low-amplitude $Ca^{2+}$ responses observed experimentally, we found that we had to use Deff = 100 $\mu m^2/s$. In the supplementary analysis, we show that an effective diffusion coefficient of this order is indeed plausible for a realistic mixture of mobile and immobile $Ca^{2+}$ buffers (Supplementary Note 2. Figure 1).

In the revised manuscript, we now provide a supplementary analysis (Supplementary Note 2) to justify this choice. Using an equation to compute the effective diffusion coefficient considering a plausible mixture of mobile and immobile buffers and an explicit reaction–diffusion model, we show that:

- The effective diffusion coefficient of $Ca^{2+}$ becomes $Ca^{2+}$ dependent, and

- There exists a regime in which low-amplitude $Ca^{2+}$ elevations are characterized by an effective diffusion coefficient of Deff = 100 $\mu m^2/s$ and a larger spatial extent than higher-amplitude transients (Supplementary Note 2. Figure 1).

Thus, the value of Deff used in the cluster model is quantitatively consistent with classical buffering theory and with plausible cytosolic buffer mixtures. This provides a mechanistic basis for the observation that small-amplitude, short-lived events can nevertheless produce coordinated signals with large spatial extent and, occasionally, almost immediate activation of $IP_3R$ clusters at distant locations in both simulations and experiments.

> *In this respect, I would also include the details of the modelling, such as implementation environment, parameters, and benchmarking. The description in the Supplementary Methods is very similar to the description in the main text. In terms of reproducibility, it would be important to at least provide simulation parameters, and providing the code would align with the emerging standards for reproducible science.*

We apologize for the lack of details of the modelling in the previous submission. In this revised version, we are providing with a full description of the model in the Supplementary Information, Note1.

To address the reviewer's request for simulations at different activation levels, we now show an additional simulation in which [$IP_3$] is higher (0.1 μM, constant in time and space) and Deff is set to 40 $\mu m^2/s$ (Supplementary Note 3). This lower effective diffusion coefficient is consistent with the stronger buffering and reduced $Ca^{2+}$ mobility expected for higher-amplitude signals. In this case, the same phenomenological cluster model generates a global $Ca^{2+}$ response with larger amplitude and longer duration, rather than a loss of activity due to excessive inhibition ((Supplementary Note 3, Figure 1, left panel). The Supplementary Note 3. Figure 1, right panel shows the 2D cell geometry, where dots indicate the random positions of $IP_3R$ clusters whose behavior is described by our phenomenological cluster model.

> *(2) Quantitative characterization of CCRICs:*
>
> *The paper would benefit from a clearer definition of the term CCRICs and quantitative descriptors like duration, amplitude distribution, frequency, and spatial extent (also in relation to the comment on the EGTA measurements below). Furthermore, it remains unclear to me whether CCRICs represent a population of rapidly propagating micro-waves or truly simultaneous events. Maybe kymographs or wave-front propagation analyses (at least from simulations if experimental resolution is too bad) would strengthen this point.*

We agree and completed the description of the CCRICs by adding:

In the Results section, p. 8, l. 27:

"…with a duration of 2.1 ± 1.0 sec (mean ± SEM) (N = 4, 128 responses)". p. 9, l. 13:

"In rare instances (less than 3%), typical local "Puff" responses elicited by these ATP concentrations could also be detected often occurring at the cell periphery (Figs. 4B, red region and 4C, red arrow; Fig. S6D, blue trace) (N > 20, cells > 500). As expected from the small concentrations of $Ca^{2+}$ released at puff sites, no increase in cytosolic $Ca^{2+}$ was detected in a distal cell region (Fig. S6D, top), indicating that isotropic $Ca^{2+}$ diffusion from a puff release site cannot account for $Ca^{2+}$ increase over large cell area. Puffs could also be detected concomitantly with CCRICs in different ROIs of the same cell (Fig. S6D, bottom). In contrast to puffs, CCRICs often showed responses of comparable amplitude in distal regions over the whole cell (Figs. 4C and S6A, B), suggesting the contribution from $IP_3R$ cluster activation by $Ca^{2+}$-Induced $Ca^{2+}$ Release (CICR). Within a given cell, the vast majority of CCRICs appeared quasi-synchronized at the fatest acquisition rate of 22 ms / frame that we could achieve. However, in few instances a delay could be detected in the elicitation of a peak in distant region of a cell (Fig. S6C). These observations suggest that the quasi-synchronization of CCRICs result from the fast diffusion of $Ca^{2+}$ leading to the activation of $IP_3R$ clusters over large cell area, which may be delayed in a some instances. Scrutinizing of CCRICs showed that while their profiles were comparable, the amplitude of these responses varied in different regions of the cell, with often a single 1 $\mu m^2$ region, likely corresponding the initial firing cluster, showing a prominent amplitude and other regions with smaller amplitude for a given response (Figs. 4B and 4C). For example, in Fig. 4C, the highest amplitude is observed in the red region for peaks 1 and 3, whereas it is observed and in the purple region for peak 2. Thus, for a given CCRIC, the respective contribution of local $IP_3R$ cluster activation and isotropic diffusion of $Ca^{2+}$from other release sites in $Ca^{2+}$ increase may vary in different regions of the cell".

In the Discussion section, 2nd sentence p. 12:

"CCRICs showed rapid kinetics with an average duration of ca 2.1 seconds and amplitude corresponding to an increase in $Ca^{2+}$ cytosolic concentration of a few hundreds nM, seemingly smaller than that of puffs (Fig. S6D), often occurring repeatedly with a frequency of up to 12 CCRICs / min over the whole cell."

We have tried to clarify the notion of coordination versus synchronization of CCRICs by showing the delay observed in some instances in the elicitation of CCRICs at distal regions of the cell, now illustrated shown in Fig S6C.

> *(3) Specificity of pharmacological tools:*
>
> *Suramin and U73122 are known to have off-target effects. Control experiments using alternative P2 receptor antagonists like PPADS or inactive U73343 analogs would strengthen the causal link.*

As suggested by the referee, we have performed complementary experiments showing the inhibitory effects of PPADS and absence of effects of U73343 on EPEC-induced Ca2+ responses including CCRICs now shown in the amended Fig. S2.

> ***Reviewer #2 (Public review):***
>
> *Summary:*
>
> *The authors of this study are trying to resolve how cellular infection by enteropathogenic E. coli (EPEC) subverts cellular signaling pathways to promote infection and dampen immune responses. Specifically, alteration in calcium dynamics has been evidenced in the prior literature as a potential initiator of these adaptations, and this study provides ideas and mechanistic detail as to how cellular calcium dynamics may be subverted by pathogens.*
>
> *Strengths:*
>
> *The clear strengths of this paper relate to the new ideas inherent in the proposed hypothesis and their support from the experimental approaches used. Overall, the proposed work provides new ideas in this area, which will benefit from further investigation. Certainly, this is an interesting and challenging paradigm to pick apart mechanistically, and is important for improving treatments from intestinal infections.*
>
> *Weaknesses:*
>
> *Additional insight is needed in three specific areas to convincingly support the conclusions drawn by the authors. These three areas are: first, a better description of the infection-associated calcium signals. Second, a mechanistic definition of the relevant purinoceptors versus other pathways to increase cellular calcium. Third, an effort to show that the proposed pathways have relevance in a polarized epithelial cell.*
>
> *(1) first, a better description of the infection-associated calcium signals.*

We agree and have added a more detailed description of the CCRICs in the results and discussion section, as detailed in response to referee 1, Weakness 2 by adding:

In the Results section, p. 8, l. 27:

"…with a duration of 2.1 ± 1.0 sec (mean ± SEM) (N = 4, 128 responses)". p. 9, l. 13:

"In rare instances (less than 3%), typical local "Puff" responses elicited by these ATP concentrations could also be detected often occurring at the cell periphery (Figs. 4B, red region and 4C, red arrow; Fig. S6D, blue trace) (N > 20, cells > 500). As expected from the small concentrations of $Ca^{2+}$ released at puff sites, no increase in cytosolic $Ca^{2+}$ was detected in a distal cell region (Fig. S6D, top), indicating that isotropic $Ca^{2+}$ diffusion from a puff release site cannot account for $Ca^{2+}$ increase over large cell area. Puffs could also be detected concomitantly with CCRICs in different ROIs of the same cell (Fig. S6D, bottom). In contrast to puffs, CCRICs often showed responses of comparable amplitude in distal regions over the

whole cell (Figs. 4C and S6A, B), suggesting the contribution from $IP_3R$ cluster activation by $Ca^{2+}$-Induced $Ca^{2+}$ Release (CICR). Within a given cell, the vast majority of CCRICs appeared quasi-synchronized at the fatest acquisition rate of 22 ms / frame that we could achieve. However, in few instances a delay could be detected in the elicitation of a peak in distant region of a cell (Fig. S6C). These observations suggest that the quasi-synchronization of CCRICs result from the fast diffusion of $Ca^{2+}$ leading to the activation of $IP_3R$ clusters over large cell area, which may be delayed in a some instances. Scrutinizing of CCRICs showed that while their profiles were comparable, the amplitude of these responses varied in different regions of the cell, with often a single 1 $\mu m^2$ region, likely corresponding the initial firing cluster, showing a prominent amplitude and other regions with smaller amplitude for a given response (Figs. 4B and 4C). For example, in Fig. 4C, the highest amplitude is observed in the red region for peaks 1 and 3, whereas it is observed and in the purple region for peak 2. Thus, for a given CCRIC, the respective contribution of local $IP_3R$ cluster activation and isotropic diffusion of $Ca^{2+}$ from other release sites in $Ca^{2+}$ increase may vary in different regions of the cell" In the Discussion section, 2nd sentence p. 12:

"CCRICs showed rapid kinetics with an average duration of ca 2.1 seconds and amplitude corresponding to an increase in $Ca^{2+}$ cytosolic concentration of a few hundreds nM, seemingly smaller than that of puffs (Fig. S6D), often occurring repeatedly with a frequency of up to 12 CCRICs / min over the whole cell."

We have tried to clarify the notion of coordination versus synchronization of CCRICs by showing the delay observed in some instances in the elicitation of CCRICs at distal regions of the cell, now illustrated shown in Fig S6C.

CRICCs are observed over the whole cell or very large cell area. We agree that this point as well as comparison with previously described puffs needed clarification. We have added the following sentences in the discussion and inserted the seminal Thomas et al. 1999 citation in the references, p. 13, l. 18:

"Consistently, while CRICCs were detected in the vast majority of cells at these very low agonist concentrations, in rare instances, local "puff-like" responses were also detected at the cell periphery. These observations are in contrast to previously described $Ca^{2+}$ puffs preceding global responses reported to occur preferentially in perinuclear area (Thomas et aL., 1999). These earlier studies, however, involved higher agonist concentrations (1-5 μM ATP) expected to lead to the release of higher $IP_3$ concentrations, which may preferentially stimulate larger $IP_3R$ clusters at the perinuclear region because of the higher density of $IP_3$ Rs. In addition, larger $IP_3$ clusters may release higher amounts of $Ca^{2+}$ for which, as opposed to CCRICs, diffusion would be restrained by $Ca^{2+}$ buffers thereby favoring the spatial confinement of the response. "

> *(2) Second, a mechanistic definition of the relevant purinoceptors versus other pathways to increase cellular calcium*

We do not believe that CCRICs are specific to EPEC, since they are also elicited by low agonist concentrations. The discrete action of Type III translocons leading to the release of small amounts of extracellular ATP at the onset of EPEC prompted us to perform fast $Ca^{2+}$ imaging at low agonists concentrations (150 nM ATP, 100 nM histamine now shown in Fig. S4), which to our knowledge, differ from higher agonist concentrations used in all previous studies describing puffs. Our modelling studies support the notion that CCRICs correspond to generic $Ca^{2+}$ release-dependent responses triggered by low levels of IP3.

We now show inhibition of CCRICs by PPADS, another purinergic receptor antagonist, and extracellular ATP depletion by addition of hexokinase in the extracellular medium in Figs. S4 and S7.

Knocking down ATP receptors represents a challenging task since HeLa cells were shown to express transcripts for most of the described 8 P2Xs and 7 P2Ys purinergic receptors (10.1016/j.bbamem.2009.03.006). Mostly, we do not believe that CCRICs are triggered by a specific ATP receptor and do not expect to see inhibition of CCRICs in single knock-down experiments. Our experimental and modelling studies suggest that CCRICs are not specific to EPEC nor to a particular ATP receptor, but instead correspond instead to generic $Ca^{2+}$ elicited at low agonist concentrations such as ATP or histamine.

Zhong et al., 2020 indeed previously showed a role for $Ca^{2+}$ influx mediated by the TRPV2 receptor in EPEC-mediated cell death. However, this influx occurred following 8 hours of cell infection with EPEC. We do not detect significant cell death or $Ca^{2+}$ influx at the onset of infection corresponding to the 12 hours infection kinetics that we used. Our experiments indicate that CCRICs do not involve $Ca^{2+}$ influx.

> *(3) Third, an effort to show that the proposed pathways have relevance in a polarized epithelial cell.*

We agree and have performed complementary experiments showing induction of CCRICs by EPEC and eATP in polarized intestinal epithelial cells, now shown in Figure S8.

> ***Recommendations for the authors:***
>
> ***Reviewer #1 (Recommendations for the authors):***
>
> *(1) Statistical treatment and data presentation:*
>
> *Some figure legends lack clarity on replicates (n = cells vs N = independent experiments). Timecourse quantifications of p-IκB and p-p65 should include normalized fold-change plots with clear statistical tests.*

To clarify, we replaced “n” by “cells”. The number of determinations and independent experiments (N) has been added in the legends to all relevant Figures and Supplementary Figures.

As requested, we now show the p-IκB and p-p65 plots as plots normalized to basal p-IκB and p-p65 levels. We mentioned in legend to Fig. 6 that we used an ANCOVA test showing significance of the effects of eATP on TNF-∝-induced IκB- and p65 phosphorylation.

> *(2) Clarification on the temperature used in imaging (why measured at 35{degree sign} C)?*

We have added the following clarification in the Materials and Methods section p. 14, l. 21:

“Imaging was then carried out at 35°C to allow for bacterial type III secretion, …”

> *(3) Figure 4A:*
>
> *The image shows a lower image acquisition interval than every 2s that is stated in the caption.*

We apologize for the mistake. The legend to Fig. 4A now reads:

“Image acquisition every 52 ms (A)…”

> *(4) Figure 4B:*
>
> *The color of ROIs could be more intense for better identification.*

We have replaced the colors of blue and green ROIs, by light cyan and purple ROIs

> *(5) Figure 4c:*
>
> *I don't understand the meaning of the dashed lines described by "The dashed red and green lines point at the aggregation of responses throughout the cell" in the caption or in the text.*

We apologize for the lack of clarity and have re-written the corresponding text p. 9, l.25 as follows:

"Scrutinization of CCRICs showed that while their profiles were comparable, the amplitude of these responses varied in different regions of the cell, with often a ca 3 $\mu m^2$ single region, likely corresponding to a source point release, showing a prominent amplitude and other regions with smaller amplitude for a given response (Figs. 4B and 4C). For example, in Fig. 4C, the highest amplitude is observed in the red region for peaks 1 and 3, whereas it is observed and in the purple region for peak 2. Thus, for a given CCRIC, the respective contribution of local IP3R cluster activation and isotropic diffusion of $Ca^{2+}$ from other release sites in $Ca^{2+}$ increase may vary in different regions of the cell."

> *(6) Figure S4A:*
>
> *The responses for EGTA are not really pointed out. Are the traces meant to show events?*

We have added arrowheads in traces corresponding to ATP + EGTA-AM treatment pointing at "flattened $Ca^{2+}$ responses". The Legend to Fig. S4A now includes the sentence: "ATP + EGTA-AM treatment led to an inhibition of $Ca^{2+}$ responses, associated with small variations in the $Ca^{2+}$ baseline, that were arbitrarily scored as flattened $Ca^{2+}$ pseudo-responses (ATP+EGTA-AM, red arrows)."

> *(7) Figure S5:*
>
> *Could not identify the purple arrow for the less mobile cluster.*

We agree that the former Figure lacked clarity and have remade Figure S5, now Figure S6, with higher magnification of panels with fast acquisition. The previously purple arrows pointing at larger and less mobile clusters are now shown in black in these enlarged panels. The legend has been changed accordingly.

> *(8) There are some typos and suboptimal formulations throughout the manuscript, such as:*
>
> *P8: "minute amount" could be changed to low, minor or similar.*

"minute" amounts of eATP was replaced by "low amounts of eATP".

> *P8: put a "%" to the numbers 61.2 {plus minus} 5.8.*

"%" was added.

> *P16: "manuscript".*

Thank you.

> ***Reviewer #2 (Recommendations for the authors):***
>
> *Suggestions relate to the following three topics.*
>
> *First, a better description of the infection-associated calcium signals. The authors emphasize throughout the paper that their imaging data challenge established concepts in the calcium signaling field (discussion). I do not see the calcium imaging data*

> *explained either with data or textually with sufficient clarity to evaluate this assertion. A start would be a clear description of the characteristics of the EPEC-evoked calcium signals relative to other local and global domains of calcium signaling previously described in HeLa cells. Prior work has shown that PI-coupled agonists evoke local calcium signals that are perinuclear in HeLa cells (PMID: 10660296), but the relationship of EPEC-evoked transients to these previously defined responses is not clear.*

We agree and have added a more detailed description of the CCRICs in the results and discussion section, as detailed in response to referee 1, Weakness 2.

> *Most importantly, it is ambiguous where in the HeLa cell recordings are made. Are these recordings close to the plasma membrane and/or deeper within the cell? The only spatial information is provided in Figure 3A, and these responses are not well described in the text or presented in a way that comparisons can be made to responses from a PI-coupled agonist.*

CRICCs are observed over the whole cell or very large cell area. We agree that this point as well as comparison with previously described puffs needed clarification. We have added the following sentences in the discussion and inserted the seminal Thomas et al. 1999 citation in the references, p. 13, l. 18:

“Consistently, while CRICCs were detected in the vast majority of cells at these very low agonist concentrations, in rare instances, local “puff-like” responses were also detected at the cell periphery. These observations are in contrast to previously described $Ca^{2+}$ puffs preceding global responses reported to occur preferentially in perinuclear area (Thomas et aL., 1999). These earlier studies, however, involved higher agonist concentrations (1-5 µM ATP) expected to lead to the release of higher $IP_3$ concentrations, which may preferentially stimulate larger $IP_3R$ clusters at the perinuclear region because of the higher density of $IP_3Rs$. In addition, larger $IP_3$ clusters may release higher amounts of $Ca^{2+}$ for which, as opposed to CCRICs, diffusion would be restrained by $Ca^{2+}$ buffers thereby favoring the spatial confinement of the response. “

> *If I understand the described responses correctly, could not these rapid local responses result from a change in cellular calcium buffering capacity consequent to infection? Are the authors proposing that these responses occur in other cells also, or represent a pathogen-specific signaling mode?*

We do not believe that CCRICs are specific to EPEC, since they are also elicited by low agonist concentrations. The discrete action of Type III translocons leading to the release of small amounts of extracellular ATP at the onset of EPEC prompted us to perform fast $Ca^{2+}$ imaging at low agonists concentrations (150 nM ATP, 100 nM histamine now shown in Fig. S4), which to our knowledge, differ from higher agonist concentrations used in all previous studies describing puffs. Our modelling studies support the notion that CCRICs correspond to generic $Ca^{2+}$ release-dependent responses triggered by low levels of IP3.

> *Second, evidence supporting a mechanistic role of ATP comes from prior literature, together with the authors' presented data showing the effects of PLC (to inhibit IP3), pharmacological inhibition (suramin, a non-selective purinoceptor blocker), and the effects of T3SS-deficient mutants (to prevent ATP release). However, there are missing steps here to mechanistically identify how ATP is working. First, does degradation of extracellular ATP (e.g., apyrase) block these responses? Second, given HeLa cells are easily amenable to knockdown approaches, does knockdown of particular ATP receptors, or TRPV2 as suggested in the prior literature, impact the calcium signal dynamics?*

We now show inhibition of CCRICs by PPADS, another purinergic receptor antagonist, and extracellular ATP depletion by addition of hexokinase in the extracellular medium in Figs. S4 and S7.

Knocking down ATP receptors represents a challenging task since HeLa cells were shown to express transcripts for most of the described 8 P2Xs and 7 P2Ys purinergic receptors (10.1016/j.bbamem.2009.03.006). Mostly, we do not believe that CCRICs are triggered by a specific ATP receptor and do not expect to see inhibition of CCRICs in single knock-down experiments. Our experimental and modelling studies suggest that CCRICs are not specific to EPEC nor to a particular ATP receptor, but instead correspond instead to generic $Ca^{2+}$ elicited at low agonist concentrations such as ATP or histamine.

Zhong et al., 2020 indeed previously showed a role for $Ca^{2+}$ influx mediated by the TRPV2 receptor in EPEC-mediated cell death. However, this influx occurred following 8 hours of cell infection with EPEC.

We do not detect significant cell death or $Ca^{2+}$ influx at the onset of infection corresponding to the 12 hours infection kinetics that we used. Our experiments indicate that CCRICs do not involve $Ca^{2+}$ influx.

> *Third, while the use of HeLa cells provides advantages for imaging and mechanistic assays, the effort to replicate findings in an intestinal cell line would heighten relevance, given the likely importance of cell type and cell polarity on the pathogen-evoked responses.*

We agree and have performed complementary experiments showing induction of CCRICs by EPEC and eATP in polarized intestinal epithelial cells, now shown in Figure S8.

https://doi.org/10.7554/eLife.108953.2.sa0